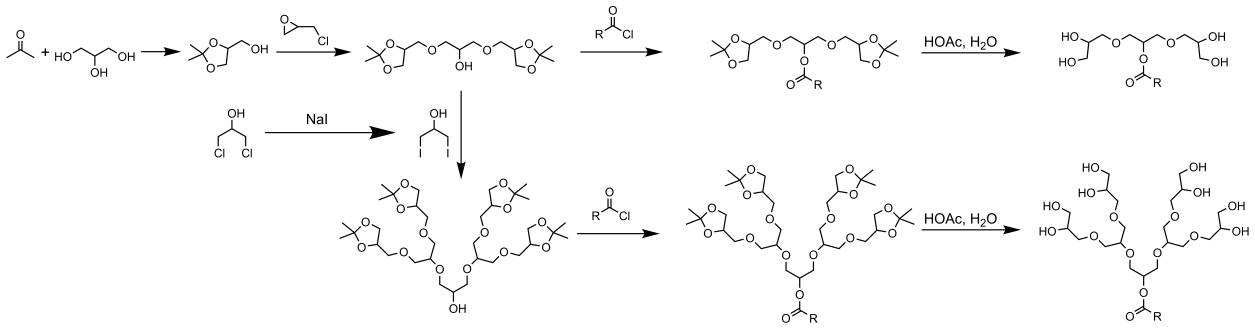

Synthesis and Characterization of Branched Polyglycerol Surfactants

Master's thesis in Materials Chemistry

Eric Moilanen

Department of Chemistry and Chemical Engineering

CHALMERS UNIVERSITY OF TECHNOLOGY
Gothenburg, Sweden 2024
www.chalmers.se

Master's thesis 2024

Synthesis and Characterization of Branched Polyglycerol Surfactants

Eric Moilanen

CHALMERS
UNIVERSITY OF TECHNOLOGY

Department of Chemistry and Chemical Engineering
Division of Applied Chemistry
Chalmers University of Technology
Gothenburg, Sweden 2024

Synthesis and Characterization of Branched Polyglycerol Surfactants
Eric Moilanen

Supervisor: Romain Bordes, Applied Chemistry
Frida Bilén, Applied Chemistry
Examiner: Lars Evenäs, Applied Chemistry

Master's Thesis 2024
Department of Chemistry and Chemical Engineering
Division of Applied Chemistry
Chalmers University of Technology
SE-412 96 Gothenburg
Telephone +46 31 772 1000

Cover: Synthesis pathway utilized in this work.

Typeset in LaTeX
Printed by Chalmers Reproservice
Gothenburg, Sweden 2024

Abstract

Polyglycerol surfactants have emerged as a promising renewable alternative to fossil based polyethylene glycol surfactants. The polyglycerol head group offers greater structural variability and possibility for functionalization. In order to facilitate the transition to renewable nonionic surfactants, a deeper understanding of the structure-property relationship, particularly regarding branching, is essential. To this end, two polyglycerol structures with different degrees of branching were synthesised through a series of chemical reactions. These structures were then esterified with carboxylate tails of varying lengths and analyzed by tensiometry, interfacial rheology and quartz crystal microbalance with dissipation monitoring. The results indicated that enlargement of the branched head group significantly influences the surfactants self-assembly and the air-water interfacial rheology. QCM-D analysis showed that the branched head group binds very strongly to hydrophilic surfaces, likely due to its hydroxylated nature.

Acknowledgement

I would like to extend my gratitude to the division of applied chemistry for providing such a welcoming atmosphere for my work. I am thankful to my supervisors, Romain Bordes and Frida Bilén, for their invaluable assistance throughout the project, from its inception to the end. A special thanks to Yiming Jia and Kinga Grenda for providing me with innovative ideas to better perform my work. Finally, I appreciate all the other masters students who contributed to a fun and friendly work environment. Thank you all!

List of Abbreviations

$CDCl_3$ - Deuterated chloroform (CAS: 865-49-6)

DCM - Dichloromethane (CAS: 75-09-2)

DMAP - N,N-Dimethylpyridin-4-amine (CAS: 1122-58-3)

DMF - N,N-dimethylformamide (CAS: 68-12-2)

MeOD - Deuterated methanol (CAS: 811-98-3)

MeOH - Methanol (CAS: 67-56-1)

TBAB - Tetrabutylammonium bromide (CAS: 1643-19-2)

$TBAHSO_4$ - Tetrabutylammonium bisulfate (CAS: 32503-27-8)

TBAI - Tetrabutylammonium iodide (CAS: 311-28-4)

TBAOH - Tetrabutylammonium hydroxide (CAS: 2052-49-5)

TFA - Trifluoroacetic acid (CAS: 76-05-1)

THF - Tetrahydryfuran (CAS: 109-99-9)

TLC - Thin layer chromatography

List of mathematical symbols

p - Pressure ($kg \cdot m^{-1} \cdot s^{-2}$)

γ - Surface tension (mNm^{-1})

g - Earth gravitational acceleration ($9.8067m \cdot s^{-2}$)

ρ - density ($kg \cdot m^{-3}$)

φ - Pendant drop tangent angle (rad)

s - pendant drop arc length (m)

Bo - Bond number (dimensionless)

r, z - pendant drop cylindrical coordinates ($kg \cdot m^{-3}$)

R_0 - Pendant drop droplet radius (m)

Γ - Surface concentration ($mol \cdot m^{-2}$)

Γ_∞ - maximum surface concentration ($mol \cdot m^{-2}$)

K_L - Langmuir constant ($L \cdot mol^{-1}$)

K_{HE} - Henry's adsorption constant ($L \cdot mol^{-1}$)

C - Concentration ($mol \cdot L^{-1}$)

h_q - QCM-D crystal thickness (m)

μ_q - QCM-D crystal shear modulus ($kg \cdot m^{-1} \cdot s^{-2}$)

ρ_q - QCM-D crystal density ($kg \cdot m^{-3}$)

f_0 - Fundamental resonant frequency (s^{-1})

C - Mass sensitivity constant ($17.7ng \cdot Hz^{-1} \cdot cm^{-2}$)

Δm_f - QCM-D crystal mass change (kg)

E_d - QCM-D energy dissipated during oscillation (J)

E_s - QCM-D energy stored in oscillation (J)

τ - QCM-D dissipation time constant (s)

Contents

List of Figures

List of Tables

1
Introduction

1.1 Background

Surfactants, amphiphilic molecules with distinct hydrophobic and hydrophilic regions, play a pivotal role in a wide variety of industrial processes and applications. They are most commonly used as detergents and cleaning agents, but also find use for other applications such as acting as foaming agents, dispersants, emulsifiers or wetting agents. The most common nonionic surfactants are based on polyethylene oxide, which is synthesized from fossil resources [1]. As the world grows more environmentally conscious, there is a growing need to replace these fossil based surfactants with surfactants made from renewable resources. One such option is polyglycerol surfactants, which can be made entirely from renewable resources. For renewable alternatives to have any real chance of replacing established and well characterized fossil resource based surfactants, the properties and characteristics of the renewable alternatives need to be better understood so as to make the transition as smooth as possible.

1.2 Aim of the study

The aim of this thesis is to increase the understanding and clarify the properties of branched polyglycerol surfactants. By synthesizing a selection of polyglycerol surfactants through selective reactions and processes, the resulting product will be of monodisperse head group size with a well-defined structure, as opposed to polydisperse and structurally random as is common with commercial nonionic surfactants. This well-defined structure will help distinguish surfactant properties which may otherwise be obscured by polydispersity, poor understanding of or variation in composition.

2
Theory

The theoretical background behind the project, the characterization methods used and the synthesis methods utilized are described in this section.

2.1 Surfactants

Surfactants play a vital role as the primary ingredient in numerous common household formulations such as detergents, washing powders, cosmetics, toothpaste and skin care products. Besides household use, they find use in nearly every industry in some fashion, from ore-flotation in the mining industry [2] to the casting of solid fuel rockets used for spacecraft [3].

2.1.1 Definition

Surfactants are amphiphilic molecules consisting of two regions with distinct properties. They consist of a polar and hydrophilic part, commonly referred to as the "head" and a nonpolar hydrophobic part referred to as the "tail" [4]. The intramolecular difference in hydrophobicity gives rise to their tendency to accumulate at interfaces, where they orient themselves as to put their distinct regions where they are energetically favored. In the case of an oil droplet in water, the hydrophobic tail finds "comfort" in surrounding itself with molecules of similar hydrophobic nature, so the surfactant molecules accumulate on the oil droplets surface with their tails facing toward the oil and head groups exposed to the surrounding water. In the lack of a favorable interface to accumulate on, the surfactant molecules find an energetically favorable solution, self-assembling into aggregates called micelles. These micelles consist of a number of surfactant molecules, often 50-100 [5], that often form a spherical shape with their tails pointed inward and heads outward in polar solvent. In a nonpolar solvent, the structure is reversed with the head groups pointed inward and tail groups outward.

2.1.2 Classification

Due to the wide variety of chemical moieties that can yield hydrophilic and hydrophobic properties, surfactants are often categorized into four general categories; anionic, cationic, zwitterionic and nonionic. This classification relates to the charge of the surfactant head group (negative, positive, both or none respectively). The reason behind classifying them by charge is due to the large effect that charge has on

their behavior and properties. Anionic surfactants are the largest of the categories in terms of volume produced. The charge carrying group is most commonly carboxylate or sulfate, but sulfonates and phosphates are also common anionic groups in these surfactants. Cationic surfactants most often have an amine carrying the positive charge. The amine can be anything from primary to quaternary in structure. Due to most solid surfaces having a negative charge, they tend to find use in applications where strong adsorption is ideal. Zwitterionic surfactants often feature amino acid derivative head groups, such as betaines and amine oxides. They tend to find use in specialty applications where the dual charge is of use. They also tend to have low skin and eye irritation which makes them suitable for personal care products. Nonionic surfactants are the second largest class of surfactants and the one explored in this work. They often have a polar head group consisting of a polyether or hydroxylated group. The most common nonionic head group is polyethylene glycol, but sugar derivatives such as glucose, sorbitans and polyglycerols also find use. [4][6]

2.2 Polyglycerol surfactants

In recent years the search for sustainable and eco-friendly alternatives to chemicals of fossil resource origin has gained significant momentum. In the case of polyethylene glycol surfactants, polyglycerol surfactants have emerged as a promising alternative both due to them being derived from renewable resources [7] and their increased functionality compared to polyethylene glycol [8]. Polyglycerol can be synthesized in a number of different ways in order to produce purely linear[8], branched[9][10] or mixed structures[11][12]. In the direct condensation of glycerol, the condensation reaction can occur on any of the 3 hydroxyl sites, resulting in a complex mixture of possible products as seen in Figure 2.1. Further complication arises from the esterification of polyglycerol, which may also occur on any of the hydroxyl groups in the polyglycerol molecules.

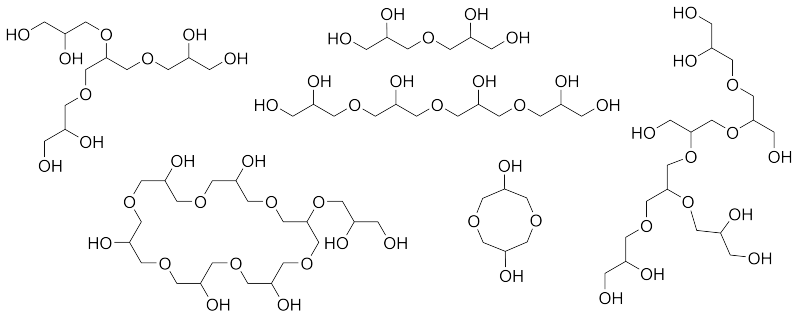

Figure 2.1: A portion of the possible polyglycerol products formed in the direct condensation of glycerol.

2.3 Surfactants synthesised in this study

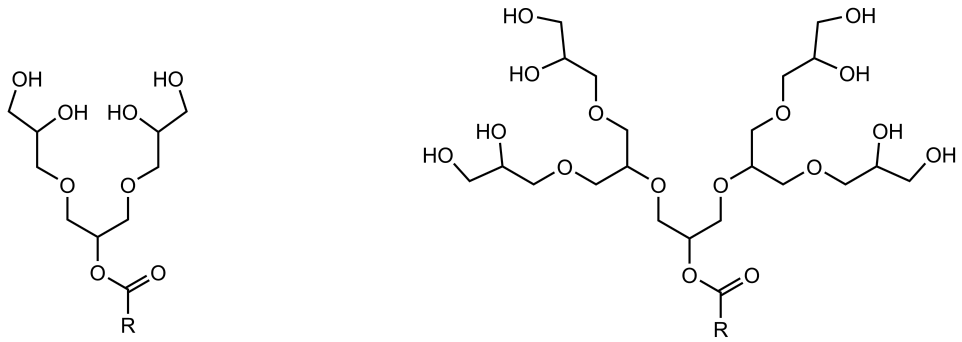

(a) Triglycerol ester **(b)** Heptaglycerol ester

Figure 2.2: Polyglycerol esters synthesised in this work. R denotes the linear carbon tail, which for the triglycerol case was 9, 11 or 13 carbon atoms long. For the heptaglycerol, the carbon tail was 13 carbon atoms long.

Two specific branched polyglycerol head groups have been synthesised and characterized in this work, the structures can be seen in Figure 2.2. Figure 2.2a shows the triglycerol head group with a single central ester bond to linear carboxylic acid. Figure 2.2b shows the heptaglycerol head group, also with a single central ester bond to a linear carboxylic acid.

2.4 Physicochemical study of the synthesised surfactants

The theoretical background behind the characterization methods used in this work are described in this section.

2.4.1 Surface tension

Surface tension is the two-dimensional analogue of pressure acting tangentially to the surface [13] that arises from the cohesive forces present in a liquid material [4]. These cohesive forces can range from extremely strong in the case of metallic bonds in liquid mercury, to very weak in the case of Van der Waals forces in liquid hydrocarbons. A simplified picture of the cohesive forces can be obtained by considering the forces enacted upon a molecule located in the bulk of a liquid and a molecule located on the surface. For a molecule located in the bulk, the forces enacted upon it are on average symmetrical and thus result in no net force. For a molecule on the surface, the asymmetry in intermolecular cohesive forces causes a net inward force, which over time results in minimization of the surface area [4]. More realistically, the lower molecular density near the surface as compared to the bulk results in surface molecules occupying a higher energy state, which similarly results in the system

seeking to minimize the energy of the surface by minimizing the surface area. [14]

The balance of internal pressure and net inward force by surface molecules is expressed in the Young-Laplace equation (Equation 2.1), where γ is the surface tension, $\Delta p = p_{external} - p_{internal}$ the pressure difference across the surface and r_1 and r_2 are the principal radii of curvature. [15]

$$\Delta p = \gamma(\frac{1}{r_1} + \frac{1}{r_2}) \tag{2.1}$$

2.4.2 Pendant drop tensiometry

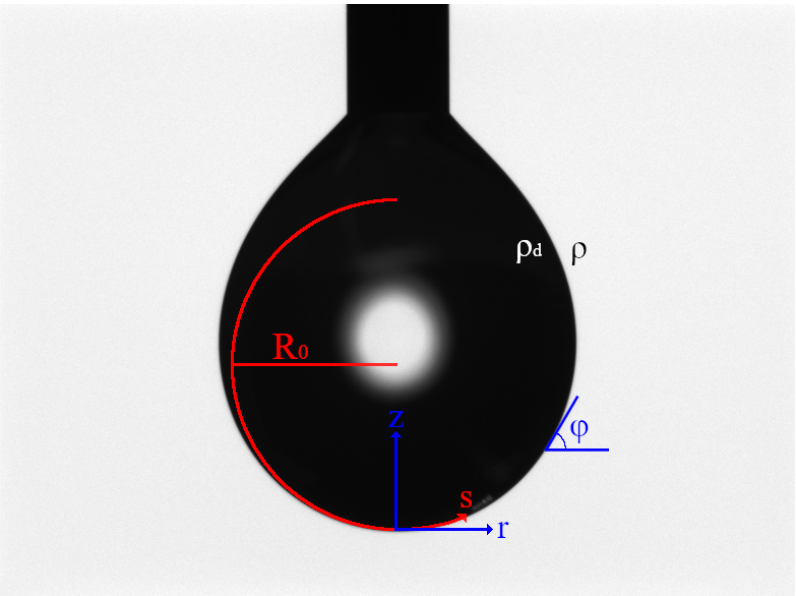

Figure 2.3: Image of a pendant drop overlaid with relevant variables discussed in this subsection.

One common method for determining the interfacial tension for liquid materials is pendant drop tensiometry. The method functions by capturing an image of a hanging droplet suspended from a needle with a digital camera and iteratively fitting the Young-Laplace equation to its shape in order to calculate the surface tension [16]. Due to gravity and the presence of the needle, the hanging droplet will not exhibit a perfectly spherical shape. It is thus necessary to use a modified Young-Laplace equation (Equation 2.2) accounting for gravity.

$$\gamma(\frac{1}{r_1} + \frac{1}{r_2}) = \Delta p = \Delta p_0 - \Delta\rho g z = \Delta p - (\rho_d - \rho)gz \tag{2.2}$$

To calculate the surface tension, the equation is written in cylindrical coordinates r, z with tangent angle φ in terms of arc length s as a set of differential equations (Equations 2.3 - 2.5) where $\bar{s}, \bar{r}$ and $\bar{z}$ scale along with the droplet radius R_0. A schematic of these coordinates and angles is shown in Figure 2.3. [17]

$$\frac{d\varphi}{d\bar{s}} = 2 - Bo\,\bar{z} - \frac{\sin\varphi}{\bar{r}} \tag{2.3}$$

$$\frac{d\bar{r}}{d\bar{s}} = \cos\varphi \tag{2.4}$$

$$\frac{d\bar{z}}{d\bar{s}} = \sin\varphi \tag{2.5}$$

By determining the value of the Bond number (Bo) and droplet radius, the interfacial tension γ can be calculated from equation 2.6.

$$\gamma = \frac{\Delta\rho g R_0^2}{Bo} \tag{2.6}$$

The differential equations may also be used to calculate the droplet volume according to equation 2.7. [17]

$$V = \pi \int \bar{r}^2 \sin\varphi d\bar{s} \tag{2.7}$$

2.4.3 Interfacial rheology by pulsating drop

The behavior and properties of a surfactant film on an interface is partially dependant on the degree of intermolecular interaction between surfactant molecules. By imparting a change to the size of the interface and observing the dynamic response it is possible to gain an understanding of the interactions occurring on the interface. [18] One method for studying the dynamics of the interface is through pulsating drop dilational interfacial rheology.

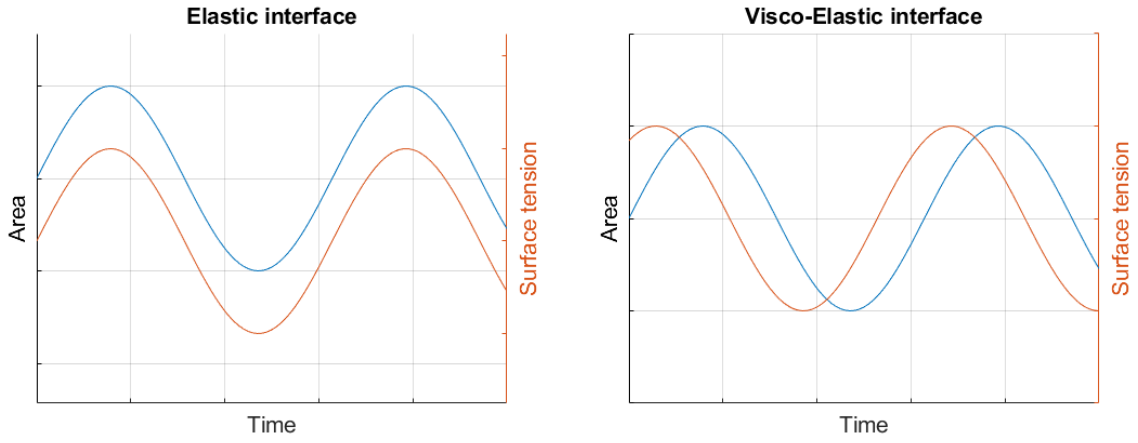

(a) Elastic interface. **(b)** Visco-elastic interface.

Figure 2.4: Illustration of the response on the surface tension of an elastic and visco-elastic interface to a sinusoidal variation in droplet size.

By varying the volume of a pendant drop in a sinusoidal manner the surface is subjected to periodic expansion and compression which induces periodic variation

in the observed surface tension with the same frequency as the induced change. In the case of a purely elastic interface, the variation in interfacial tension will occur in phase with the change in surface area and volume, as seen in Figure 2.4a. In the case of visco-elastic interface the observed surface tension response will be delayed compared to the induced change, this can be observed as a phase shift when plotting the area and surface tension as seen in Figure 2.4b. [19][20]
As surfactant molecules adsorb to an interface they reach an equilibrium interfacial concentration which depends on factors such as bulk concentration, size of the surfactant molecule, composition of the phases and nature of the surfactant. When an interface at equilibrium is expanded, the system will seek to restore the now lower interfacial concentration (observed as a higher than equilibrium surface tension) to equilibrium by adsorption of molecules from the bulk to the interface. If the interface is contracted, the higher than equilibrium interfacial concentration (seen as a lower than equilibrium surface tension) will induce desorption of surfactants. The rate at which surfactants can adsorb onto and desorb from the interface depends on the mobility of the surfactant, the bulk concentration and interfacial energy [20]. A strong intermolecular interaction between surfactant molecules at the surface results in a longer delay in desorption due to the higher energy needed to break the intermolecular bonds.

2.4.4 Adsorption at solid surfaces

The adsorption of surfactants at solid surfaces is governed by the energetically favorable formation of a solution-surfactant-solid interface as well as the hydrophobic effect. When studying the phenomenon, the adsorption process is often analyzed through the adsorption isotherm, which relates the surface concentration of a solute to its bulk concentration. [4]
There are numerous models that have been developed for modelling the isotherm, ranging from simple linear relationships such as "Henry's adsorption isotherm" [21] to complex models such as the 5 parameter Fritz–Schlünder isotherm which can accurately model the adsorption behavior over a wide range experimental data [22]. Perhaps the most well known isotherm model is the Langmuir adsorption isotherm (Equation 2.8) [23][24], which relates the surface coverage of an adsorbate Γ as a function of the adsorbate concentration C, the maximum surface coverage Γ_∞ and the Langmuir constant K_L. While simple, the model is based on kinetic principles and accounts for the fact that there is finite surface area onto which the surfactant can adsorb as a monolayer. The further simplified Henry's adsorption isotherm (Equation 2.9) assumes a linear relationship of concentration and surface coverage by Henry's adsorption constant K_{HE} and does not account for a finite surface. As seen in Figure 2.5, the model is only valid at low surface coverage.

$$\Gamma = \frac{\Gamma_\infty K_L}{1 + K_L C} \tag{2.8}$$

$$\Gamma = K_{HE} C \tag{2.9}$$

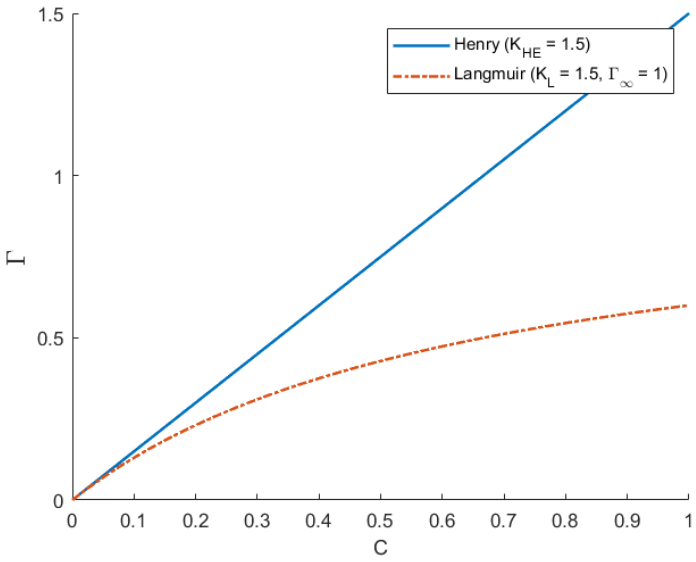

Figure 2.5: Examples of Henry's isotherm and Langmuir isotherm.

2.4.5 Quartz Crystal Microbalance with Dissipation monitoring (QCM-D)

Quartz Crystal Microbalance with Dissipation monitoring (QCM-D) is a method of monitoring and measuring the adsorption of chemicals such as surfactants or polymers at solid surfaces. The method relies on oscillating a carefully cut and sized quartz crystal by the piezoelectric effect at its resonance frequency, which depends on the thickness of the the crystal by Equation 2.10, where n is the overtone number and equal to $1, 3, 5, 7...$, h_q is the thickness of the crystal, μ_q is the shear modulus of the crystal, ρ_q is the density of the crystal and f_0 is the crystals fundamental resonant frequency. [25]

$$nf_0 = \frac{n}{2h_q}\sqrt{\frac{\mu_q}{\rho_q}} \tag{2.10}$$

If the thickness of the resonating crystal is increased by deposition of material onto its surface, the new thickness h_q' will change the resonant frequency to a new frequency f_q' by Equation 2.11. [25]

$$\Delta f = f_q' - f_q = \frac{n(h_q' - h_q)}{2h_q' h_q}\sqrt{\frac{\mu_q}{\rho_q}} \tag{2.11}$$

When the deposited material is rigidly adsorbed as a very thin layer ($h_q' - h_q << h_q$) the change in frequency can be expressed in terms of the mass change of the crystal Δm_f by the Sauerbrey equation 2.12. C is the mass sensitivity constant which is approximately equal to 17.7 ng $cm^{-2}Hz^{-1}$ for a 5 MHz quartz crystal.[25][26]

$$\Delta m_f = -\frac{\rho_q h_q}{f_0}\frac{\Delta f}{n} = -C\frac{\Delta f}{n} \tag{2.12}$$

It is worth noting that the linear relationship between the frequency shift Δf and mass change Δm_f is only truly valid in air or vacuum. If the crystal is surrounded by a Newtonian medium such as water, the surrounding medium will dampen the oscillation. If the dampening effect is large enough, the linear relationship will no longer be valid. The dampening effect can be expressed as the dissipation factor D through Equation 2.13 where E_d is the dissipated energy during an oscillation and E_s is the energy stored in the oscillating crystal. [25][27]

$$D = \frac{E_d}{2\pi E_s} \tag{2.13}$$

In real terms, a large dissipation factor corresponds to a soft and swollen layer adsorbed on the surface and a small dissipation factor corresponds to a hard and dense adsorbed layer. The dissipation may be observed and measured by removing the driving voltage from the system and monitoring the amplitude of the voltage generated from the crystal as the oscillation decays. If a sinusoidal function (Equation 2.14) is fit to the decaying output voltage, the dissipation time constant τ may be extracted and used to calculate the dissipation factor D through Equation 2.15, where A(t) is the amplitude of the oscillating potential signal over time, A_0 is the starting amplitude, f is the oscillating frequency, φ is the phase of the oscillating signal and t is the time [25].

$$A(t) = A_0 e^{-t/\tau} \mathrm{Sin}(2\pi f t + \varphi) + C \tag{2.14}$$

$$D = \frac{1}{\pi f \tau} \tag{2.15}$$

In the case that the dissipation factor is large and so the relationship between frequency shift Δf and mass change Δm_f is no longer linear, the Voigt model may be applied to obtain Δf and ΔD [27]. The treatment of the data for this purpose is considerably complex and will not be explored in this work.

2.5 Reaction theory

The mechanisms of the chemical reactions utilized in this work are described in this section.

2.5.1 Acid catalyzed ketal synthesis

The acid catalyzed reaction between an alcohol and a ketone or aldehyde produces ketals and acetals respectively through a 7 step mechanism. If performed without active removal of water formed in the reaction, the reaction will reach an equilibrium point dependant on the stoichiometry and reaction conditions. For ketals, the equilibrium constant is often quite small, ranging from $0.021 \cdot 10^{-3}$ for cyclopentadecanone to $0.65 \cdot 10^{-3}$ for acetone in anhydrous methanol [28].

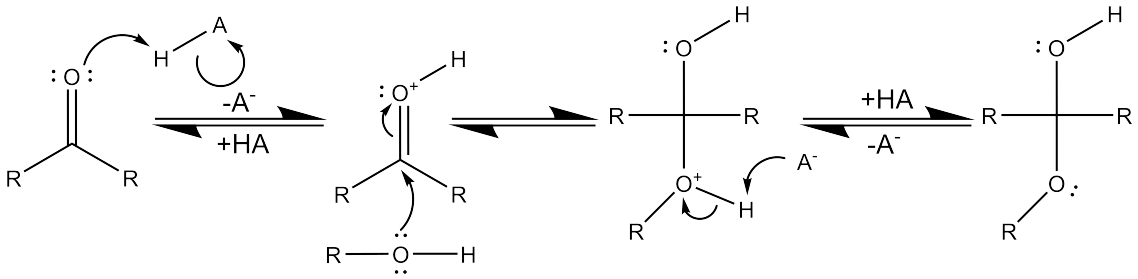

Figure 2.6: Acid catalyzed formation of hemiacetal.

In the first step of the reaction mechanism, illustrated Figure 2.6 above, the oxygen of the carbonyl is protonated, creating a more electrophilic carbon centre which is subsequently attacked by a lone pair on the alcohol oxygen. The formed adduct is then deprotonated, producing a hemiacetal and reforming the acid catalyst.

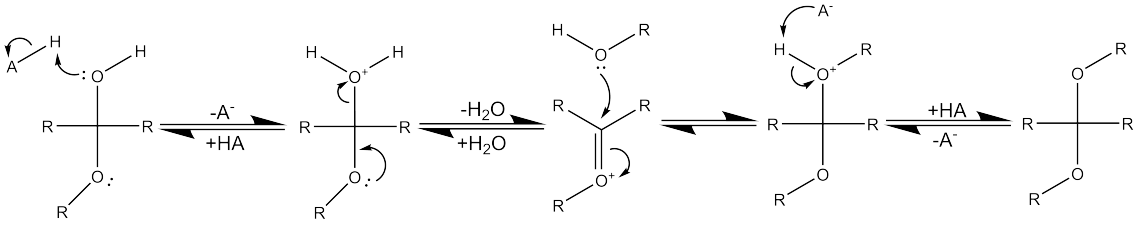

Figure 2.7: Acid catalyzed formation of ketals.

In the next step, illustrated in Figure 2.7, the hydroxyl group of the formed hemiacetal is protonated by the acid catalyst, forming the $^{+}OH_2$ moiety, an excellent leaving group for the subsequent electron shift in which the lone pair on the ether bond oxygen forms a double bond and kicks off a molecule of water. The electrophilic oxonium intermediate is then attacked by the lone pair on a second alcohol molecule. The created intermediate is then again deprotonated, reforming the acid catalyst and producing the final ketal or acetal product. [29]

2.5.2 Epichlorohydrin coupling

The reaction between epichlorohydrin and alkoxides is relatively complex, having multiple different competing pathways that produce two possible products.

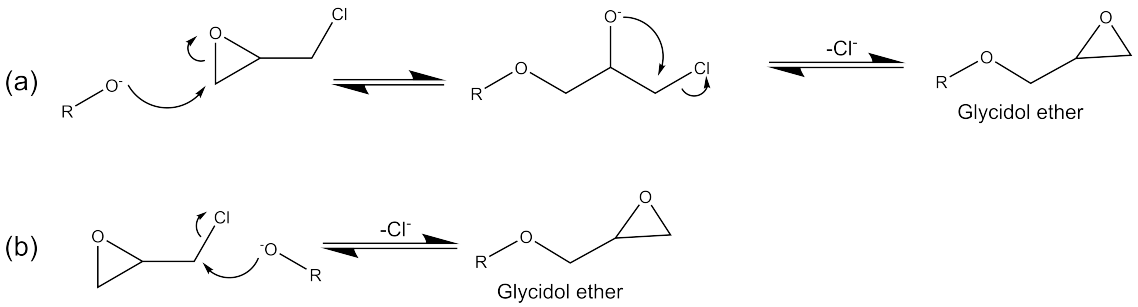

Figure 2.8: Mechanisms of glycidol ether formations by addition of alkoxide to epichlorohydrin.

The coupling of alkoxide by epichlorohydrin may follow two pathways, both of which are illustrated in Figure 2.8. In pathway (a), the alkoxide reacts with the epoxide ring by S_N2 ring opening nucleophilic addition. The formed halohydrin intermediate then undergoes a ring closing intramolecular reaction, kicking off chloride. In pathway (b), the alkoxide nucleophile attacks the exposed carbon atom, again kicking off chloride [29]. Regardless of the pathway, the formed glycidol ether product is the same.

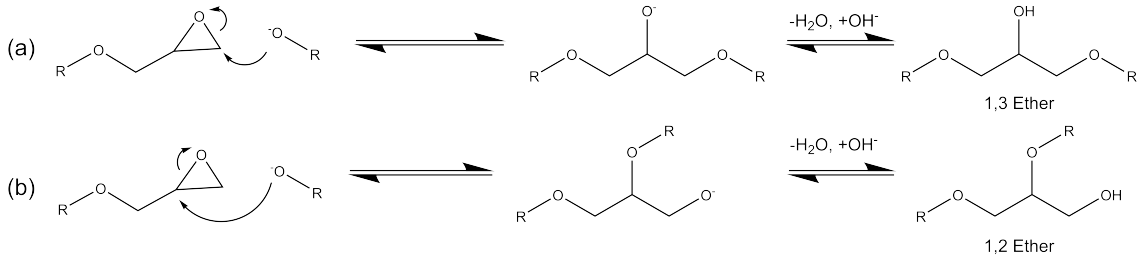

Figure 2.9: Mechanistic pathways of reaction between glycidol ether and alkoxide.

A second alkoxide coupling may occur on either side of the epoxide but is sterically favored to occur on the exposed end illustrated in path (a) in Figure 2.9 [30]. The mechanism is the same as the first coupling, but due to the lack of a good leaving group the oxygen of the opened ring is unable to close into a ring and remains deprotonated until the workup, in which it finally forms a 1,3 or 1,2 glycerol ether depending on which side of the epoxide was reacted.

2.5.3 DMAP catalyzed acid chloride esterification

Esterfication of alcohols by acid chlorides are commonly mediated by performing the reaction in a basic amine solvent such as triethylamine or pyridine [29]. In the case of pyridine catalysis, the reaction is sometimes named as the "Einhorn acylation" [31]. The reaction can be enhanced by the addition of a more reactive amine such as 4-dimethylaminopyridine (DMAP). [32]

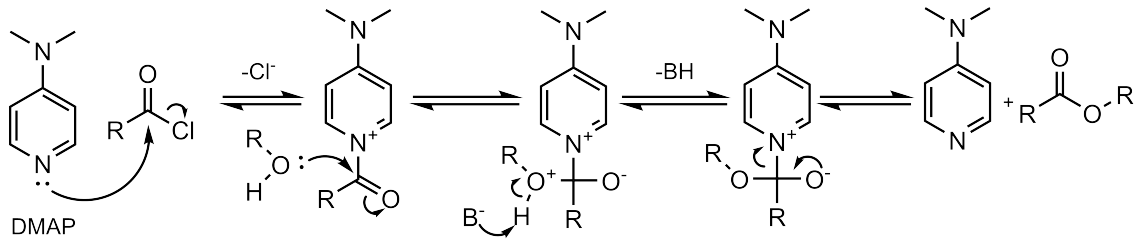

Figure 2.10: Mechanism of DMAP catalyzed acid chloride esterification.

The first step of the reaction is a nucleophilic attack by the nitrogen on the pyridine ring on the carbonyl carbon of the acid chloride, forming a more electrophilic intermediate. The carbonyl subsequently undergoes nucleophilic addition by the alcohol, forming a tetrahedral intermediate which is deprotonated by a base (amine

solvent or another molecule of DMAP). The tetrahedral intermediate then undergoes an intramolecular electron shift, reforming the carbon-oxygen double bond and regenerating the DMAP catalyst. [29][31]

3
Method

The synthesis methods for the preparation of the surfactants as well as the methods for their characterization by tensiometry, interfacial rheology and QCM-D are described in this chapter.

3.1 Synthesis

The procedures used for the synthesis of the characterized surfactants are described in this section. All flash column chromatography described was performed using silica gel 60. All thin layer chromatography (TLC) described was performed on aluminium backed silica gel 60 plates, stained with an alkaline solution of potassium permanganate to visualise the spots and developed by heating with a hot air gun.

3.1.1 Solketal

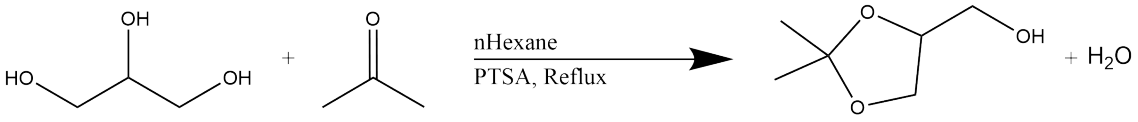

Figure 3.1: Reaction of glycerol with acetone under acidic condition.

Into a 500 ml roundbottom flask was added 37.1 g glycerol (0.403 mol, 1 equiv), 1.2324 g p-toluenesulfonic acid monohydrate (6.5 mmol, 0.016 equiv) (PTSA), 108 ml acetone (1.46 mol, 3.62 equiv) and 108 ml n-Hexane. The flask was equipped with a 100 ml Soxhlet apparatus charged with 55 g dry 4Å molecular sieves. The mixture was then refluxed overnight. In order to neutralize p-toluenesulfonic acid, 1.05 g sodium acetate (0.0128 mol, 0.0318 equiv) was added to the room temperature reaction mixture and stirred for 20 min. The mixture was filtered and evaporated to dryness, yielding 54.1337 g dark brown crude solketal. The crude solketal was further purified by vacuum distillation (16 mbar) yielding 46.2909 g colorless solketal (0.350 mol, 87%). ^{1}H NMR (600 MHz, $CDCl_3$) δ 4.23 (tdd, J = 6.5, 5.2, 3.7 Hz, 1H), 4.03 (dd, J = 8.2, 6.6 Hz, 1H), 3.78 (dd, J = 8.2, 6.5 Hz, 1H), 3.72 (ddd, J = 11.6, 5.7, 3.7 Hz, 1H), 3.58 (ddd, J = 11.6, 6.5, 5.2 Hz, 1H), 2.04 (t, J = 6.2 Hz, 1H), 1.43 (s, 3H), 1.36 (s, 3H). ^{13}C NMR (151 MHz, $CDCl_3$) δ 109.41, 76.14, 65.70, 63.01, 25.27. FTIR (neat): v 3433 (OH), 2986, 2939, 2881, 1456, 1371, 1256, 1211,

1155, 1120, 1070, 1046, 985, 969, 911, 877, 839, 792, 731, 651, 625, 592, 515, 471, 421 cm-1. RI (21.6°C) 1.43565

3.1.2 Triglycerol ketal

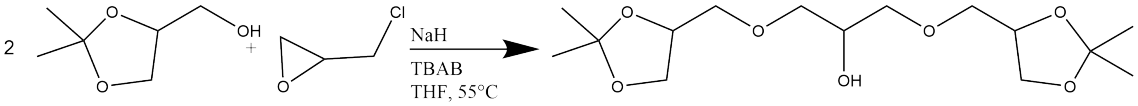

Figure 3.2: Alkoxide mediated reaction of solketal with epichlorohydrin.

Under a nitrogen, in 250 ml roundbottom flask was added 4.5446 g 60 wt% sodium hydride (NaH) dispersion in mineral oil (114 mmol, 2.48 equiv) and 75 ml tetrahydrofuran (THF). The mixture was then stirred to suspend the sodium hydride. The suspension was cooled by brine and ice bath, made by spreading approximately 50 g of sodium chloride onto 500 ml crushed ice and filling with water to cover the ice. Once cool, 12.6 ml solketal (101 mmol, 2.2 equiv) was slowly added over 10 min. 308.7 mg tetrabutylammonium bromide (TBAB) (0.958 mmol, 0.02 equiv) and 3.6 ml epichlorohydrin (45.9 mmol, 1 equiv) were added. After approximately 20 minutes, the mixture was heated to 55 °C for 55 hours. Next, the mixture was evaporated to dryness and dissolved into a mixture of 100 ml water and 120 ml dichloromethane (DCM). The organic phase was separated and the aqueous phase was extracted with 3x80 ml DCM. The combined organic phase were dried over sodium sulfate then evaporated to dryness. Product was purified by vacuum distillation using Schlenk line vacuum (unknown pressure). Composition and distillation temperature range of 3 obtained fractions are presented in Table 3.1 below. Obtained triglycerol ketal and mineral oil mixture was transferred to a vial and left to stand overnight to settle. The heavier triglycerol ketal phase was extracted by needle and washed with 1 ml n-hexane, then evaporated to dryness, yielding 4.0699 g light yellow triglycerol ketal (12.7 mmol, 27.7%) ^{1}H NMR (600 MHz, Chloroform-d) δ 4.27 (dq, J = 11.9, 6.1 Hz, 2H), 4.04 (ddt, J = 8.1, 6.5, 1.9 Hz, 2H), 3.96 (ttt, J = 8.8, 4.2, 2.0 Hz, 1H), 3.75 – 3.69 (m, 2H), 3.55 (dtddd, J = 71.9, 18.7, 16.9, 13.0, 7.2, 4.2 Hz, 8H), 2.73-2.64 (dt, J = 2.69, 1 H) ii, 1.42 (s, 6H), 1.35 (s, 6H). ^{13}C NMR (151 MHz, $CDCl_3$) δ 109.53, 74.70, 72.75, 72.50, 69.45, 66.54, 26.75, 25.38. FTIR (neat): v 3471 (OH),2986, 2936, 2871, 1479, 1456, 1380, 1371, 1325, 1253, 1212, 1144, 1078, 1049, 975, 935, 841, 733, 668, 647, 573, 514, 426 cm-1. RI (21.7°C) 1.457665

Table 3.1: Distillation range and composition of obtained fractions from distillation of triglycerol ketal.

Fraction	Distillation range	Composition
1	50-55 °C	Solketal
2	55-120 °C	Solketal with trace triglycerol ketal
3	120-175 °C	Triglycerol ketal and mineral oil

3.1.3 Esterification and deprotection of triglycerol ketal

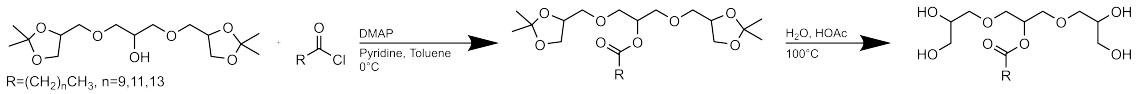

Figure 3.3: Esterification and deprotection of triglycerol ketal.

Into a 25 ml round bottom flask was added 1 g triglycerol ketal (3.123 mmol, 1 equiv), 5 ml pyridine and 25 mg DMAP (0.205 mmol, 0.0655 equiv). The mixture was then cooled by ice bath. Acid chloride, see Table 3.2, dissolved in 10 ml toluene was slowly added to the cooled mixture and stirred for 2.5 hours. The reaction mixture was diluted with 10 ml water and extracted with 4x30 ml diethylether. Combined ether phase was washed with 10 ml 1 M hydrochloric acid, 10 ml saturated sodium bicarbonate solution and 10 ml brine. The washed ether phase was dried over sodium sulfate and evaporated to dryness. The product was isolated by flash column chromatography using 4:1 hexane:ethyl acetate. Fractions containing the ester product were combined and evaporated to dryness, see Table 3.3 for yields. Purified triglycerol ketal ester was dissolved in a mixture of 9.4 ml glacial acetic acid and 2.4 ml water. The mixture was heated to 100 °C by oil bath and stirred for 1.5-2h while monitoring the progress by TLC using pure ethyl acetate as eluent. The acetic acid mixture was then evaporated to dryness and product isolated by flash column chromatography using pure ethyl acetate eluent. Yields of the three esters are presented in Table 3.3 below.

Table 3.2: Acid chlorides used for esterification and the amounts used.

Acid chloride	Amount
Decanoyl chloride (C10)	0.84 ml (0.772 g, 4.05 mmol, 1.3 equiv)
Dodecanoyl chloride (C12)	0.94 ml (0.889 g, 4.06 mmol, 1.3 equiv)
Tetradecanoyl chloride (C14)	1.1 ml (0.998 g, 4.05 mmol, 1.3 equiv)

Table 3.3: Yields of the protected and deprotected esters.

Ester tail	Ketal protected ester	Deprotected ester
C10	1.1800 g (2.479 mmol, 79.6%)	0.5426 g (1.376 mmol, 55.5%)
C12	0.6668 (1.33 mmol, 42.5%)	0.2487 g (0.588 mmol, 44.3%)
C14	1.1428 g (2.153 mmol, 68.9%)	0.6611 g (1.468 mmol, 68.2%)

3.1.4 1,3-diiodo-2-propanol

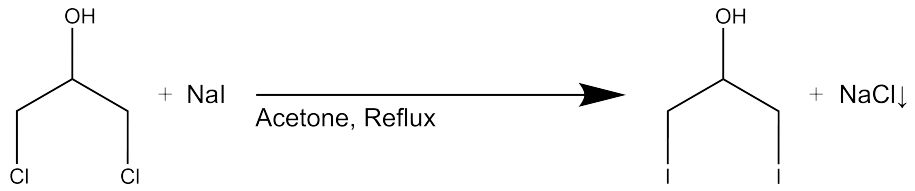

Figure 3.4: Transhalogenation of 1,3-dichloro-2-propanol.

Into a 50 ml round bottom flask equipped with a Liebig condenser was added 9.5 g sodium iodide (63.38 mmol, 4 equiv), 1.5 ml 1,3-dichloro-2-propanol (2.0445 g, 15.85 mmol, 1 equiv) and 20 ml acetone. The mixture was refluxed for 71 hours. The reaction mixture was then filtered to remove sodium chloride formed by the reaction and evaporated to dryness. Next, the product was dissolved in 50 ml diethyl ether as to precipitate remaining sodium iodide, then filtered and evaporated to dryness yielding 4.5688g crude 1,3-diiodo-2-propanol. The evaporated product was used directly for subsequent steps without further purification. By the mass of sodium chloride and potassium iodide removed in the filtration steps, the apparent conversion was between 88-92.4 %.

3.1.5 Heptaglycerol ketal

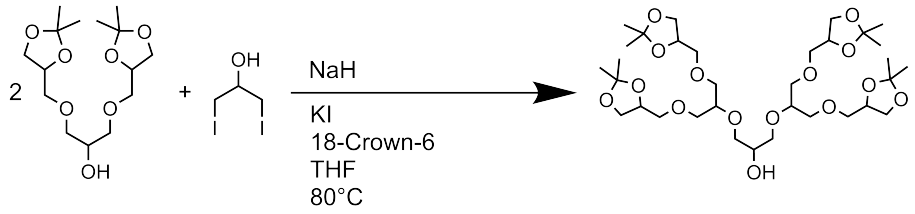

Figure 3.5: Coupling of triglycerol ketal using 1,3-diiodo-2-propanol.

Into a 100 ml two neck round bottom flask was charged 0.5531 g 60 wt% sodium hydride dispersion in mineral oil (13.8 mmol, 3.29 equiv) and 12.5 ml 10 mg/ml 18-Crown-6 in THF (0.47 mmol, 0.11 equiv). The mixture was stirred to suspend the sodium hydride. Next, 3.0012 g triglycerol ketal (9.37 mmol, 2.24 equiv) in 28 ml THF was added. The mixture was stirred at room temperature for 10 minutes, then a condenser attached and mixture refluxed for 1 h. After refluxing, 0.5 g potassium iodide (3.01 mmol, 0.72 equiv) and 1.3083 g 1,3-diiodo-2-propanol (4.19 mmol, 1 equiv) in 5 ml THF was added dropwise to the refluxing mixture over 15 minutes. Reaction was maintained at reflux using an oil bath for 68.5 hours, then left to cool to room temperature. Once cool, 18 ml water was added and the mixture evaporated to dryness. The dried reaction mix was dissolved into a mixture of 20 ml brine, 10 ml water and 20 ml DCM. The organic phase was separated and the aqueous phase extracted with 6x100 ml ethyl acetate. The combined organic extracts were combined and dried over sodium sulfate then evaporated to dryness.

The crude product was purified by flash column chromatography using pure ethyl acetate eluent. Yield: 0.4134 g heptaglycerol ketal (0.594 mmol, 14%) ^{1}H NMR (600 MHz, $CDCl_3$) δ 4.29-4.2 (m, 4H), 4.07-4.01 (t, 4H), 3.92-3.82 (m, 1H), 3.75-3.44 (m, 29H), 1.45-1.38 (s, 12H), 1.38-1.31 (s, 12H) ^{13}C NMR (151 MHz, $CDCl_3$) δ 109.39, 79.25, 78.69, 78.45, 74.61, 72.51, 72.29, 71.98, 70.56, 69.75, 66.79, 26.80, 25.44. m/z = 714.4256 C33H60O15NH4+ (calculated = 714.427599)

3.1.6 Heptaglycerol ketal esterification and deprotection

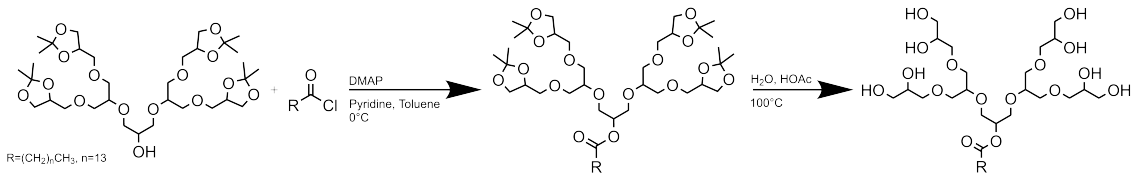

Figure 3.6: Esterification and deprotection of heptaglycerol ketal.

Into a 10 ml round bottom flask was charged 0.4134 g of the previously prepared heptaglycerol ketal (0.594 mmol, 1 equiv), 3 ml pyridine and 28.4 mg DMAP (0.232 mmol, 0.4 equiv). The mixture was stirred on ice. Once cool, a mixture of 0.2 ml tetradecanoyl chloride (0.736 mmol, 1.24 equiv) in 2.5 ml toluene was added dropwise. The flask was stoppered and left to stir for 20.5 h at 0°C. Next, the mixture was diluted with 3 ml water and extracted with 6x30 ml diethyl ether. The combined ether phase was washed with 3 ml of 1.2 M HCl, 3 ml saturated sodium bicarbonate solution and 3 ml brine. The ether phase was then dried over sodium sulfate and evaporated to dryness. Crude product was purified by flash column chromatography using 4:1 hexane:ethyl acetate. Yield: 0.5509 g (0.607 mmol, 102%). The purified ketal protected ester was deprotected by dissolving the product in a mixture of 4 ml glacial acetic acid and 1 ml water and refluxing the mixture for 120 minutes. Progress of the deprotection was monitored by TLC using 1:1 methanol:ethyl acetate. When no notable change occurs in the TLC, the reaction was taken off heat and evaporated to dryness. Purification of the crude product was attempted by flash chromatography using 1:1 ethyl acetate:methanol, resulting in poor yield of fully deprotected ester contaminated with a large proportion of heptaglycerol. Yield: 39 mg impure ester. ^{1}H NMR (600 MHz, MeOD) δ 3.81-3.73 (m, 307H) 2.34-2.27 (t, 1H) 1.65-1.54 (m, 2H) 1.37-1.24 (m, 22H) 0.93-0.87 (t, 3H) ^{13}C NMR (151 MHz, MeOD) δ 80.13, 79.78, 73.98, 72.80, 72.67, 72.32δ, 72.21, 71.02, 64.48, 34.83, 30.78, 24.26, 14.46.

By NMR, based on the fact that the heptaglycerol moiety contains 35 non labile hydrogen atoms and the C14 carbon tail contains 22 hydrogen atoms in the δ 1.37-1.24 range, the concentration of heptaglycerol C14 ester in the mixture was calculated from Equation 3.1 to be 11.4% which corresponds to a yield of 0.006%.

$$\frac{\mathrm{H_{Heptaglycerol}}}{\mathrm{H_{Tail}}} = \frac{35\mathrm{x} + 35(1-\mathrm{x})}{22\mathrm{x}} \tag{3.1}$$

3.2 Other attempted synthesis methods

Some of the synthesis procedures attempted during the synthesis phase of the study are described in this section.

3.2.1 Triglycerol ketal using aqueous KOH

Into a 50 ml round bottom flask was added 8.6244 g Solketal (65.3 mmol, 3 equiv), 2.9645 g 85 wt% KOH (45 mmol, 2.07 equiv), 1.1133 g water and 0.7087 g 40 wt% tetrabutylammonium hydroxide (TBAOH) (1.10 mmol, 0.05 equiv). The flask was plugged with a septum and set to stir in an oil bath set 55 °C for 30 minutes. 1.7 ml epichlorohydrin (21.7 mmol, 1 equiv) was slowly added dropwise over 10 minute. The mixture was left to stir in the heated oil bath for 42 hours. The flask was removed from heat and diluted with 45 ml saturated sodium bicarbonate solution. The diluted mixture was then extracted with 3x20 ml ethyl acetate. Combined organic phase was dried over sodium sulfate, then evaporated to dryness. Crude product was purified by flash column chromatography using 20:1 DCM:MeOH eluent. Yield: 0.21 g brown triglycerol ketal (0.66 mmol, 3%).

3.2.2 Esterification by triethylamine and deprotection by TFA+MeOH

Into a 10 ml round bottom flask was added 0.5 g triglycerol ketal (1.56 mmol, 1 equiv), 2.5 ml DCM, 0.395 g triethylamine (3.9 mmol, 2.5 equiv). The mixture was stirred in ice bath and 0.854 g dodecanoyl chloride (3.9 mmol, 2.5 equiv) was added drop wise over 15 minutes. The mixture was stirred on ice for 1 h, then diluted with 2.5 ml DCM. The diluted reaction mixture was washed with 2 ml water, 2x1.5 ml brine. Combined aqueous washings were extracted with 5 ml DCM. Combined DCM phases were washed with 2 ml water, dried over sodium sulfate and evaporated to dryness. Yield: 1.21 g crude triglycerol ketal C12 ester. 1.16 g of the crude product was dissolved in a mixture of 1:3 trifluoroacetic acid:methanol (TFA:MeOH) by volume and left to stand for 2 days. The reaction mixture was evaporated to dryness and purified using flash column chromatography using ethyl acetate eluent. Yield: 0.1324 g (0.313 mmol, 20% over 2 steps.)

3.2.3 Coupling of solketal with 1,3-dichloro-2-propanol

Into a 150 ml round bottom flask was added 0.293 g 60 wt% sodium hydride (7.4 mmol, 3.43 equiv) and 80 ml THF. The mixture was cooled by ice and 0.57 ml solketal (4.58 mmol, 2.1 equiv) added. The mixture was stirred on ice for 45 minutes. 0.2 ml 1,3-dichloro-2-propanol (2.16 mmol, 1 equiv) was added along with 6 ml 10 mmol/ml 18-Crown-6 and 100 mg KI. The ice bath was exchanged for an oil bath, and the mixture heated to 50 °C for 18.5 h. The reaction mixture was removed from the oil bath and cooled to room temperature. 4 ml water was added and the mixture evaporated to dryness. The dried reaction mixture was dissolved in a mixture of 20 ml brine, 20 ml water and 40 ml DCM. The DCM phase was separated and the

aqueous phase extracted with 3x30 ml ethyl acetate. The combined organic phases were dried over sodium sulfate and evaporated to dryness. TLC of crude product confirms formation of triglycerol ketal.

3.2.4 Coupling of triglycerol ketal using 1,3-diiodo-2-propanol and potassium carbonate

Into a 100 ml round bottom flash was charged 1.0073 g triglycerol ketal (3.12 mmol, 2.18 equiv), 3.2403 g dry potassium carbonate (23.4 mmol, 16.36 equiv) and 25 ml DMF. The mixture was heated in an 80 °C oil bath for 30 minutes. 0.4450 g 1,3-diiodo-2-propanol (1.43 mmol, 1 equiv) was added dropwise over 10 minutes. Temperature of the oil bath was increased to 100 °C and 0.26 g potassium iodide added. Mixture was left to stir 21 h. The reaction mixture was diluted with 100 ml water, extracted with 6x30 ml DCM and 30 ml ethyl acetate. Combined organic phase was dried over sodium sulfate and evaporated to dryness. Crude product was purified by flash column chromatography using 1:1 methanol:ethyl acetate eluent. Yield: 27.2 mg heptaglycerol ketal (0.039 mmol, 2.7%)

3.3 Characterization

The methods used to characterize the synthesised surfactants were described in the following section.

3.3.1 Pendant drop tensiometry

Solutions of the triglycerol C10, C12 and C14 ester as well as the heptaglycerol C14 ester were prepared initially as 1 wt% stock solution in Milli-Q water subsequently diluted to create logarithmic concentration series. The concentration series were later completed with further points according to initial crude estimate of CMC, the complete list of concentrations is presented in Table 3.4.

Table 3.4: Weight concentrations of triglycerol and heptaglycerol esters measured for determining CMC.

3GlyC10	3GlyC12	3GlyC14	7GlyC14
1%	1%	1%	1%
0.1%	0.1%	0.1%	0.9%
0.06%	0.01%	0.01%	0.7%
0.02%	0.007%	0.007%	0.2%
0.01%	0.004%	0.004%	0.1%
0.009%	0.002%	0.002%	0.07%
0.007%	0.001%	0.001%	0.02%
0.004%		0.0001%	0.01%

Pendant drop interfacial tensiometry measurements were performed with a Biolin Scientific Attension Theta optical goniometer with 6-8 measurements per solution.

45 seconds was allowed for stabilization of the droplet. Once stabilized, the droplet was recorded by the apparatus for 2 seconds at 15 frames per second, mean surface tension during the recording calculated by OneAttension software (version 2.6.0.0).

3.3.2 Pulsating drop interfacial rheology

Based on the results obtained from pendant drop tensiometry, three concentrations of each surfactant were prepared in Milli-Q water below the determined CMC value. The concentrations used were presented in Table 3.5.

Table 3.5: Concentrations of triglycerol and heptaglycerol esters measured for interfacial rheology.

3GlyC10	3GlyC12	3GlyC14	7GlyC14
0.002%	0.0015%	0.0015%	0.002%
0.01%	0.002%	0.002%	0.07%
0.04%	0.004%	0.00625%	0.2%

Pulsating drop interfacial rheology measurements were performed with a Biolin Scientific Attension Theta optical goniometer with piezoelectric pulsator. 30 seconds was allowed for the hanging droplet to stabilize and a further 15 seconds for the pulsing to stabilize after initialization of the pulsing. The droplets were recorded for 20-30 seconds with 38-75 frames per second. For each concentration, pulsing with frequencies of 0.1 Hz, 0.2 Hz, 0.4 Hz, 0.6 Hz, 0.8 Hz, 1.0 Hz and 1.2 Hz were recorded. Surface tension at each frame of the captured recording was calculated by OneAttension software version 2.6.0.0. Custom Matlab code was used to fit sinusoidal equations to the acquired data. The surface tension data was fit to Equation 3.2 and surface area data was fit to Equation 3.3 to extract the phase of the measured oscillation. In these equations, A is the amplitude of the oscillating signal, Hz is the frequency of the oscillation, φ is the phase of the oscillating signal, $N_0e^{-t*\tau}$ and $Y-mt$ are correction factors for the exponential and linear decrease in the oscillating signals. The phase shift was subsequently calculated in degrees by Equation 3.4.

$$f(t) = ASin(t2\pi Hz + \varphi_{surfacetension}) + N_0e^{-t*\tau} \tag{3.2}$$

$$f(t) = ASin(t2\pi Hz + \varphi_{area}) + Y - mt \tag{3.3}$$

$$\text{phase shift (deg)} = -(\varphi_{area} - \varphi_{surfacetension})\frac{360}{2\pi} \tag{3.4}$$

3.3.3 QCM-D adsorption on solid interfaces

QCM-D measurements were performed on the triglycerol C10 and C12 ester on hydrophobically modified gold surfaces and for the triglycerol C10 on hydrophilically modified gold surfaces. A 1 wt% stock solution of the esters was used to create a

series of 8 concentrations, 5 below the determined CMC value and 3 above. The concentrations used are presented in Table 3.6. For the modifications to work correctly, the surfaces were cleaned by an initial 10-20 minute treatment in a UV-Ozone oven, followed by a 5 minute oxidative cleaning in a 70 °C mixture of 10 ml Milli-Q water, 2 ml 25% aqueous ammonia and 2 ml 30% hydrogen peroxide. Immediately after the cleaning the surfaces were rinsed with Milli-Q water and dried with N_2 gas to remove cleaning solution residues. For the hydrophobic surface modification, the freshly cleaned surfaces were treated overnight in a 2 mM solution of hexadecanethiol in pure ethanol, followed by rinsing with ethanol and water and drying with N_2 gas. Hydrophilic modification was performed in the same manner using a 2 mM solution of 16-mercaptohexadecanol in pure ethanol.

Table 3.6: Concentrations used for QCM-D measurements of triglycerol C10 and C12 surfactants.

3GlyC10	3GlyC12
1%	1 wt%
0.6%	0.2%
0.3%	0.02%
0.13%	0.01%
0.07%	0.006%
0.04%	0.003%
0.02%	0.002%
0.01%	0.001%

The QCM-D measurements were performed using a 4 cell Biolin Scientific QSense quartz crystal microbalance using QSoft software version 2.5.8.527 with a ISMATEC ISM935C peristaltic pump to flow the surfactant solutions over the surfaces. Before injection of the surfactant solutions, the resonant frequencies of the quartz crystal surfaces were found in air and then in Milli-Q water to confirm their functionality. Before injection of the surfactant solutions, Milli-Q water was continuously injected in order to observe potential drift in the measured ΔF and ΔD. The solutions were then injected in increasing concentration order with approximately 10 minutes of measurement for each concentration. Once the highest concentration had been measured, the system was rinsed with Milli-Q water and continuously measured in order to evaluate the desorption of the surfactant from the modified surface. The acquired ΔF and ΔD vs time data was then exported using QTools software version 3.0.7.230 and processed using custom Matlab code to adjust the data for the drift observed during the initial Milli-Q water flow and calculate the adsorbed mass based on Equation 2.12.

4

Results & discussion

The results of the synthesis work as well as the characterization studies performed are discussed in this chapter.

4.1 Synthesis

The synthesis of triglycerol esters with tail lengths of 10, 12 and 14 carbon atoms as well as heptaglycerol with 14 carbon atom long tail is discussed in this section. Other attempted synthesis as well as problems encountered during the syntheses are also discussed.

4.1.1 Solketal

The procedure of the solketal synthesis was adapted from the descriptions given by Yao et. al. [33] and Krief et. al. [34], with the modifications of utilizing a Soxhlet apparatus filled with sieves for the sequestering of water from the mixture as seen in Figure 4.1. The product was also purified by distillation as opposed to column chromatography due to the scale of the reaction. The obtained yield of 87% was slightly below the quantitative yields described by Yao and Krief. The purity of the product as confirmed by ^{1}H (Appendix Figure 7.2) and ^{13}C (Appendix Figure 7.3) NMR and FTIR spectroscopy (Appendix Figure 7.1) was excellent.

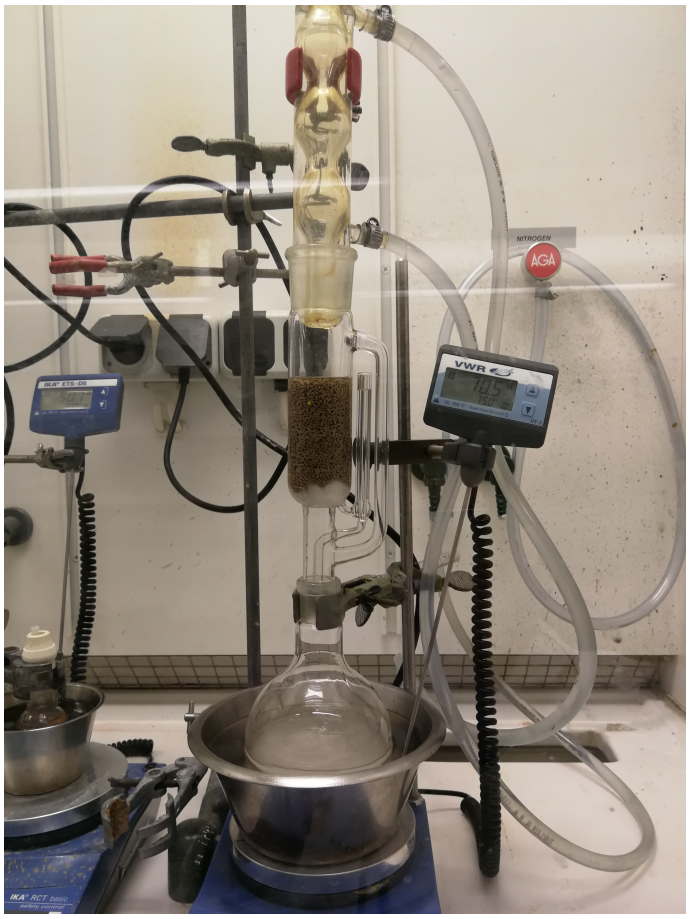

Figure 4.1: Setup used for the synthesis of solketal.

4.1.2 Triglycerol ketal

Several approaches to the synthesis of triglycerol ketal were attempted before settling on the final method described in this work. Based on the work of Bucher and Gilmour [10], synthesis utilizing sodium hydride to generate the solketal alkoxide and TBAB as catalyst for the coupling was attempted. The reason for using TBAB catalyst is not made clear in Bucher and Gilmours work, but it seems likely that the goal is to facilitate the Williamson ether synthesis reaction by exchange of the epichlorohydrin chloride into bromide. This theory is supported by the use of KI and 18-crown-6 in similar coupling reactions using solketal [9]. The synthesis resulted in a low yield of 25-33% compared to their stated 73%. Several attempts at this reaction were made with little improvement to the result, varying the amount of solvent, temperature and addition speed of epichlorohydrin had little to no impact on the obtained yield.
One issue encountered during the synthesis attempts in THF with sodium hydride was the formation of seemingly polymeric side products, potentially formed by the product 1,3-ether-alkoxide reacting with the intermediate glycidol ether. During one attempt, the crude product obtained after workup formed a blockage in the silica column which was resolved by heating and addition of DCM but resulted in poor separation and low yield. After encountering the blockage issue, all future

attempts at the synthesis were purified by vacuum distillation as described in other works [35][36]. The purification by vacuum distillation was comparatively easy and seemed to result in higher yields due to not needing any washings in the workup stage. The purity of the product obtained this way was fair as seen by the FTIR (Figure 7.4), ^{1}H (Figure 7.5) and ^{13}C (Figure 7.6) NMR results.
We finally settled on the approach utilized the preparation outlined by Bucher and Gilmour with the modification of purifying the product by vacuum distillation instead of column chromatography. The issue of comparatively low yield was mitigated for subsequent steps by increasing the scale of the reaction with the expectation of only obtaining around 25% yield. A possible reason for the low yield is the solidification of the reaction mixture shortly after addition of the epichlorohydrin. The solidified reaction mixture slowly loosens and darkens over time and returns to a fluid suspension after 24-48 hours as seen in Figure 4.2. This observation seems to not be discussed in any literature on the subject, but could explain the low yields observed due to the reagents not mixing properly for a large portion of the reaction time.

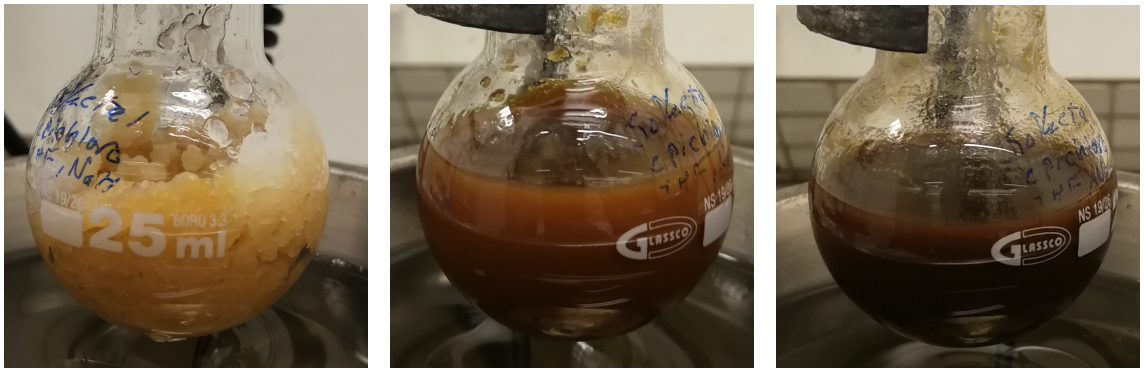

(a) Shortly after mixing. **(b)** After 24h. **(c)** After 50h.

Figure 4.2: Progression of the solketal coupling reaction in THF using sodium hydride.

Coupling under aqueous conditions was attempted as described in a patent [37], with the seemingly minor change of using TBAOH instead of TBAI. The reaction resulted in a poor yield of <1.9% in heavily contaminated black paste form. The replacement of TBAI to TBAOH was done under the impression that TBAOH is the active catalyst, due to its indirect use in other works where it is formed *in situ* from $TBAHSO_4$[38].

4.1.3 Heptaglycerol ketal

The synthesis of heptaglycerol ketal in literature is generally performed by Williamson ether synthesis using 3-chloro-2-chloromethyl-1-propene followed by subsequent ozonolysis and reduction with sodium borohydride as seen in Figure 4.3. The complex procedure seems to result in a wide range of yields from around 5.5 to 94% [39][36][40]. Due to the dangerous nature of ozone and lack of equipment needed to create and

handle substantial amounts of it, the method was deemed impossible to utilize.

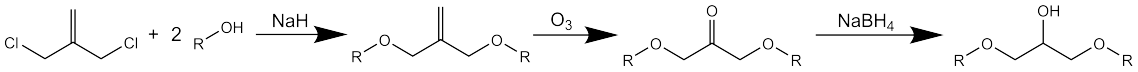

Figure 4.3: Heptaglycerol synthesis using 3-chloro-2-chloromethyl-1-propene.

Based on literature references on couplings of short to long alcohols by 1,3-dichloro-2-propanol [41][42][43] it was decided to attempt the coupling of solketal in similar fashion. The reaction was attempted in small scale using THF solvent and catalyzed by KI with 18-crown-6 in a similar manner as for the 3-chloro-2-chloromethyl-1-propene procedures [39][40]. The reaction showed formation of triglycerol ketal by TLC and it was thus attempted in the same way with the more precious triglycerol ketal. This time, the reaction showed no formation of a coupled product. It was decided, based on the use of KI catalysis to convert the 1,3-dichloro-2-propanol to its corresponding diiodide by Finkelstein reaction. The conversion procedure proceeded in a textbook fashion with apparent conversion around 90%. When the coupling reaction was attempted with the diiodide the target heptaglycerol was formed in 14% yield with decent purity as indicated by ^{1}H (Appendix Figure 7.17) and ^{13}C (Appendix Figure 7.18) NMR. Due to the reagent triglycerol ketal and product heptaglycerol ketal having very similar NMR shifts, the formation of the product was further confirmed by mass spectrometry as seen in Figure 7.19.

Due to the low yield, another method of coupling using DMF and potassium carbonate based on the work of Wang et. al. [44] was attempted. The procedure resulted in a 2.5% yield. Due to time constraints, no further options or conditions for the coupling were explored before settling on the described method.

4.1.4 Esterification and deprotection of polyglycerol ketals

Due to the ketal protecting group being labile in the presence of water and acid, a water-free esterification method had to be used for the synthesis to ensure esterification on the correct location on the polyglycerol head group. The use of acid chlorides in water free solvent under alkaline conditions is therefore an obvious choice due to its relatively high yield under mild temperature conditions. Initially, esterification of triglycerol ketal using dodecanoyl chloride in DCM with triethylamine was attempted. This reaction resulted in the formation of strongly colored side products as seen in Figure 4.4, likely due to the formation of ketene by triethylamine deprotonating the acid chloride on its alpha position [45].

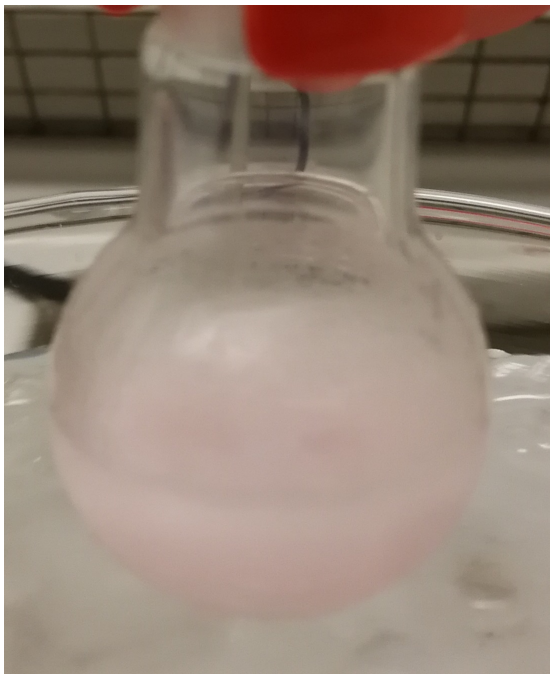

(a) Initial appearance after mixing reagents.

(b) After stirring for 24h.

Figure 4.4: Esterification of triglycerol ketal using triethylamine in DCM.

Due to the issue encountered when using triethylamine as the base, the reaction was attempted with the weaker base pyridine instead. DMAP was also added as catalyst due to the high yields described in literature in its use for similar esterifications [32][46]. In all attempts when using DMAP and pyridine, no strong color change was observed during the course of the reaction. The yields obtained for the ester products were acceptable although below what was expected, in the range of 42.5-79.6% for the triglycerol ketal, and seemingly close to quantitative for the heptaglycerol ketal. The higher yield in the heptaglycerol ketal esterification is most likely due to allowing the reaction to run for 20 hours instead of 2.5 hours. ^{1}H NMR (Appendix Figures 7.7, 7.9, 7.20) and ^{13}C (Appendix Figures 7.8, 7.10, 7.21) for the obtained ketal protected esters were consistent and indicated good purity.
The deprotection of the ketal protected esters was initially attempted by reaction with TFA and methanol as described in some literature [39][47]. Due to the small amount of literature on the subject and the poor yield obtained in the attempt, it was instead opted to deprotect the ketal esters in a mixture of acetic acid and water. The results of this were were yields in the range of 44.3-68.2 % for the triglycerol esters and 0.0006% for the heptaglycerol C14 ester. The dramatically lower yield of the heptaglycerol ester was product of the separation issue in its purification. The difference in polarity between the product formed from incomplete deprotection, complete deprotection and hydrolysis is very small (see Figure 4.5). The flash column chromatography was only able to poorly separate the mixture, so the majority of product eluted from the column overlapping with ester still containing ketal protecting groups. This fraction could not be used for characterization, as the still protected ester is surface active and would likely interfere with the results. The

obtained fraction containing no ketal protecting groups was severely contaminated with heptaglycerol formed from hydrolysis (See Figures 7.22 and 7.18), however the surface activity of this contaminant should be negligible so the sample was used for characterization. The purity of the triglycerol esters as shown by ^{1}H (Figures 7.11, 7.13, 7.15) and ^{13}C (Figures 7.12, 7.14, 7.16) was good and no separation issue was encountered in the purification of these.

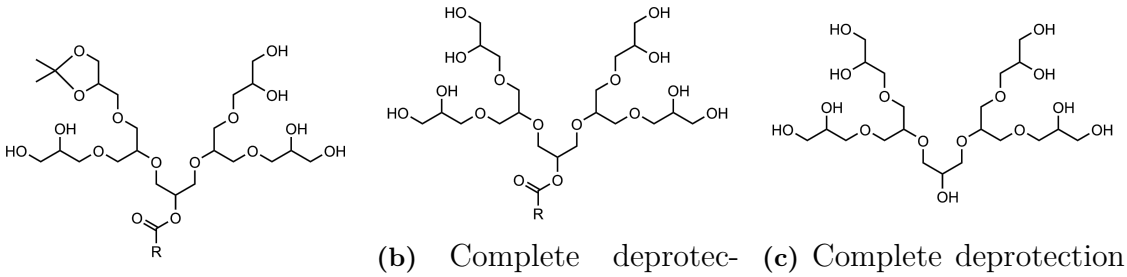

(a) Partial deprotection.

(b) Complete deprotection.

(c) Complete deprotection and hydrolyzed ester bond.

Figure 4.5: Heptaglycerol products obtained in the deprotection of heptaglycerol ketal ester.

4.2 Physicochemical study

The results acquired by pendant drop tensiometry, interfacial rheology by pulsating drop and QCM-D are discussed in this section.

4.2.1 Pendant drop tensiometry

The pendant drop tensiometry results showed significant decrease in surface tension for all measured surfactants. Figure 4.6 shows the concentration vs surface tension plot for triglycerol esters C10, C12 and C14 measured at ambient temperature 21°C. The curves exhibit the expected trend of linearly decreasing surface tension followed by a sharp transition to a plateau at the critical micelle concentration. The order of the CMC values also follow the expected trend of decreasing with increased hydrophobic contribution from the longer alkyl chains.

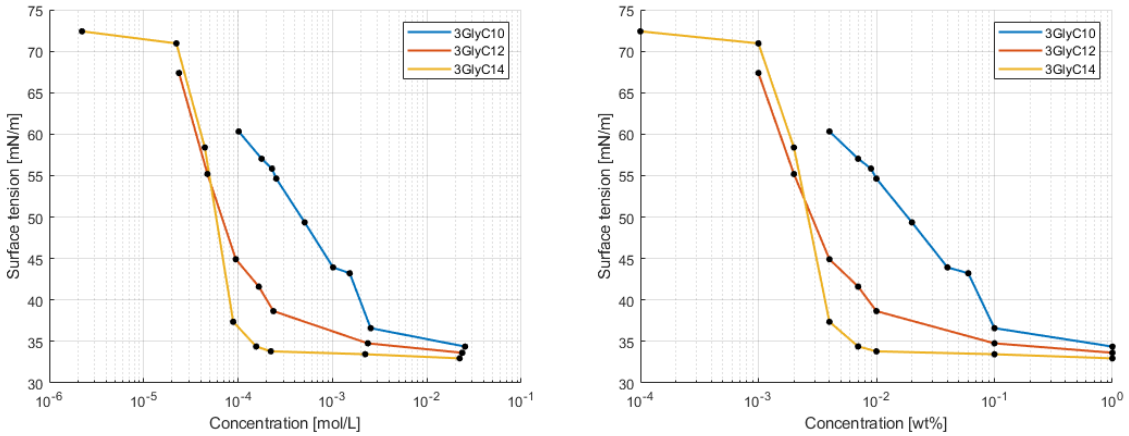

(a) Concentration in mol/L. **(b)** Concentration in wt%.

Figure 4.6: Surface tension vs concentration of triglycerol esters C10, C12 and C14.

When linear regression was performed on the decreasing sections and the plateau sections of the curves as shown in Figure 4.7 , the intercept indicating the CMC point could be determined. The CMC points as well as the area per molecule calculated form the slope of the decreasing region are presented in Table 4.1. Here the results also follow the expected trend of decreasing area per molecule with increasing hydrophobic contribution to the surfactant. It should however be noted that the calculated values for area per molecule for the C12 and C14 ester are substantially below what is generally expected for nonionic surfactants.

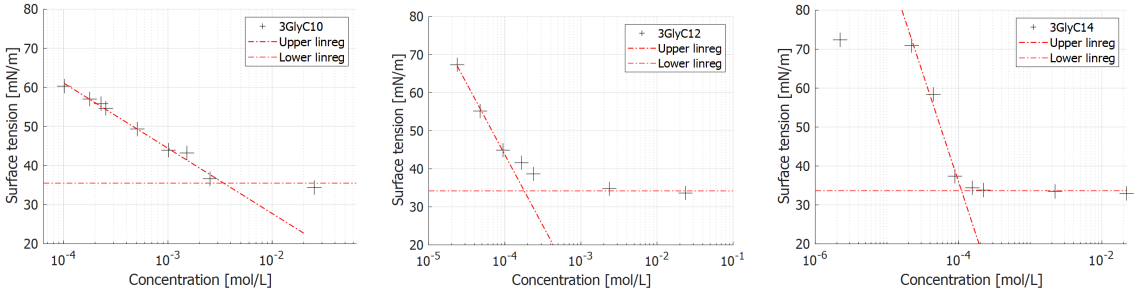

(a) Triglycerol C10. **(b)** Triglycerol C12. **(c)** Triglycerol C14.

Figure 4.7: Surface tension vs concentration triglycerol C10, C12 and C14 esters with linear regressions.

Table 4.1: CMC and area per molecule determined for the triglycerol surfactants.

	3GlyC10	3GlyC12	3GlyC14
CMC [mmol/L]	3.43	0.18	0.11
Γ [µmol/m^2]	2.96	6.63	9.90
A [Å^2]	56.0	25.1	16.8

Due to the poor separation in the purification heptaglycerol C14 ester, the solutions created with it were severely contaminated with non-esterified heptaglycerol. Interpretation of its CMC point therefore has to be done under the assumption that the heptaglycerol contamination does not affect the self-assembly of the ester nor its adsorption to the air-water interface. This assumption is likely realistic, since the heptaglycerol is extremely hydrophilic and should therefore not have any significant driving force to adsorb to the interface and interact with the heptaglycerol C14 ester. Based on the surface tension results seen in Figure 4.8, the CMC point appears to be 0.847 mmol/L, this value may be inaccurate to some degree due to the mentioned contamination and low yield preventing creation of solutions at higher concentrations to better confirm the location of the plateau. The calculated excess surface concentration and area per molecule, seen in Table 4.2, are substantially different from the values obtained for the triglycerol C14 ester. The larger area per molecule is most likely an effect of the much larger headgroup.

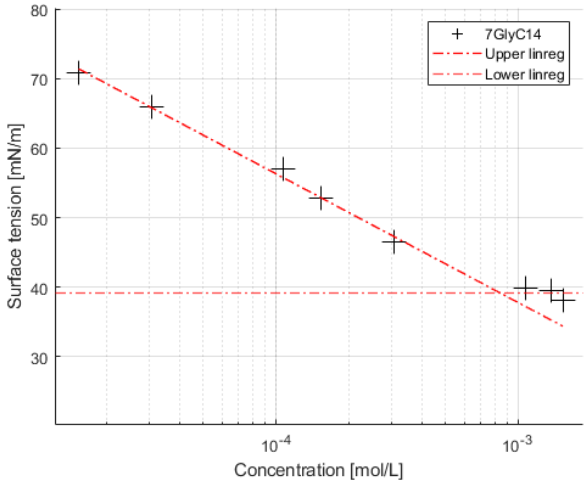

Figure 4.8: Surface tension vs concentration heptaglycerol C14 ester with linear regressions. Note that the concentration here has been adjusted with consideration for the purity of the sample used.

Table 4.2: CMC and area per molecule determined for heptaglycerol C14 ester.

	7GlyC14
CMC [mmol/L]	0.847
Γ [mmol/1000m^2]	3.28
A [Å^2]	50.54

4.2.2 Pulsating drop interfacial rheology

The interfacial rheology measurements using the Attension Theta optical goniometer were complicated by the lack of enclosure to the droplet which resulted in a high level of noise in the surface tension measurement. Occasional perturbances in the room would cause wild oscillations in the surface tension results and require

the measurement to be restarted, an example of this can be seen in Figure 4.9a. Additionally, due to a pressure leak somewhere in the system the size of the droplet would decrease rapidly, far faster than shrinkage due to evaporation, preventing measurements longer than 30 seconds. These issues resulted in the lowest frequency being reasonable to measure being 0.1 Hz, as smaller frequencies require proportionally longer recording duration to ensure accurate fitting of the sinusoidal function. For most measurements, the created Matlab program was able to accurately fit the required functions to the data. An example of this can be seen in Figure 4.9b. The results of the automated fitting was inspected for accuracy by eye, making adjustments to the starting points of the step-wise optimizing fitting function as needed.

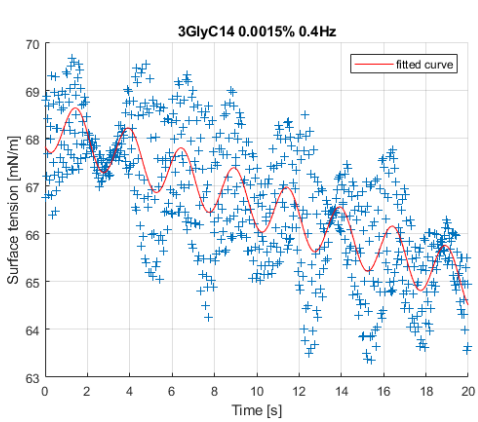

(a) An unused measurement with a large degree of noise.

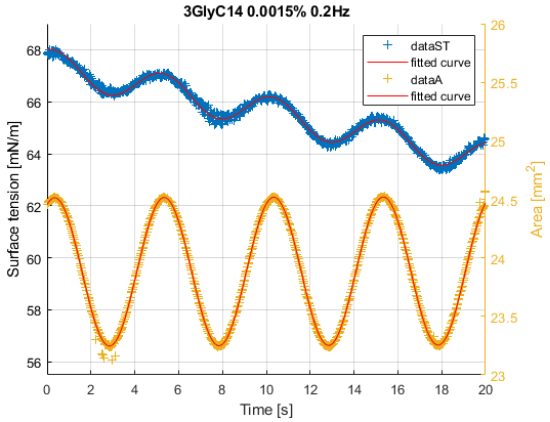

(b) An example of measurement with low noise and well fitting functions.

Figure 4.9: Surface tension vs concentration of triglycerol esters C10, C12 and C14.

Observing the results for the triglycerol C10 ester, shown in Figure 4.10a, it can be seen that there is a small decrease in phase shift with increasing frequency for the 0.002% and 0.01% samples. The 0.04% sample seems to exhibit a counterintuative increasing trend. The generally expected result is a decrease in phase shift with increased frequency, as the higher frequencies should give less time for the surface to reach equilibrium and cause maximum delay in the surface tension oscillation. For the C12 ester, Figure 4.10b, there is no similar increase in phase shift for the concentration closest to CMC. Instead, the phase shift decreases for all concentrations with increasing frequency. The results also show a larger phase shift with increasing concentration, which was expected due to the higher concentration resulting in a higher surface concentration. A higher surface concentration is expected to result in larger phase shift due to the intermolecular interactions between the surfactants giving rise to increased visco-elastic character to the surface. The results from the C14 ester, seen in Figure 4.10c, show a large degree of noise in the measurements; however, it can still be seen that for the lowest concentration 0.0015% there is no substantial phase shift at any frequency. This is somewhat strange given that the C12 ester shows a fairly large phase shift at similar concentration. The result can however be explained by the low surface concentration at 0.0015% concentration,

if the trend seen in Figure 4.6b is extrapolated toward lower concentrations, the concentration corresponds to a surface tension of approximately 65 mN/m. This high value of surface tension corresponds to a low surfactant surface concentration which may have prevented substantial intramolecular interactions from occurring and causing a phase shift to occur.

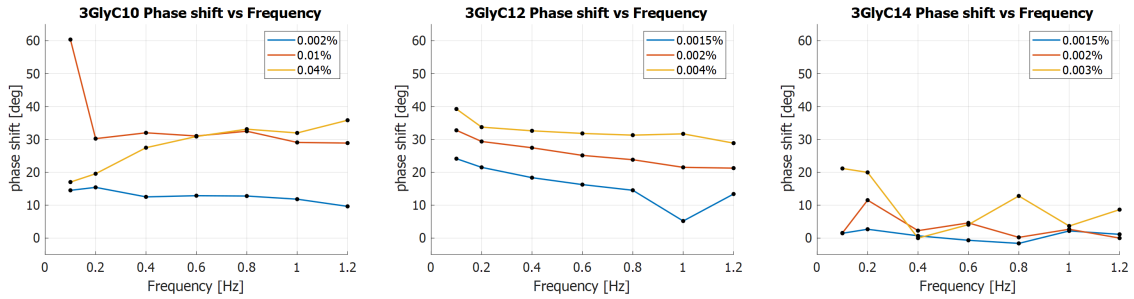

(a) 3GlyC10 **(b)** 3GlyC12 **(c)** 3GlyC14

Figure 4.10: Phase shift vs frequency for triglycerol esters C10, C12 and C14.

The heptaglycerol C14 ester exhibited similar results to the triglycerol C12 ester as seen in Figure 4.11, albeit with a larger degree of noise. Further observing the figure, it can be seen that the phase shift is significantly larger for the whole frequency range than it is for the triglycerol C14 ester. This result could be interpreted as confirmation of stronger intermolecular interaction at the surface.

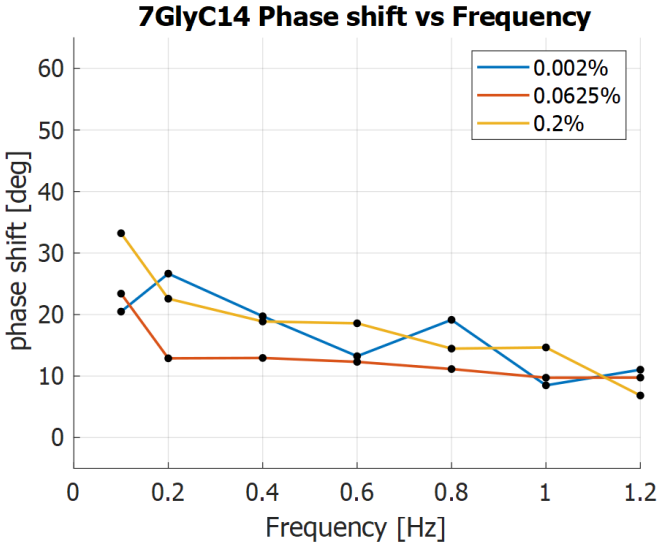

Figure 4.11: Phase shift vs frequency for heptaglycerol C14 ester.

4.2.3 Adsorption at solid surfaces using QCM-D

During the planning phase of the thesis project, it was hypothesized that due to the strong hydrophilic nature of the polyglycerol head group the surfactants would strongly adhere to hydrophilic surfaces. It was also hypothesized that the adsorption on hydrophilic surface would allow for the formation of a surfactant double

layer. In order to investigate the adsorption behavior, the surfactants were analyzed by QCM-D on both hydrophobic and hydrophilic surfaces in order to observe the difference.

Before further analysis of the acquired data, the ΔF and ΔD vs time data was adjusted for drift by fitting a line function to the initial measurement of water and subsequently subtracting the line function from the data. The result of this adjustment is shown in Figure 4.12. As can be observed in the figure, the frequency shift during the last section of the plot, corresponding to the rinsing step using pure water, is above 0 even after adjusting for drift. According to Equation 2.12, an above 0 frequency shift corresponds to a loss off mass on the sensor. This could be due to an air bubble, loss off surface modification or if the drift was not linear. The latter explanation seems most likely.

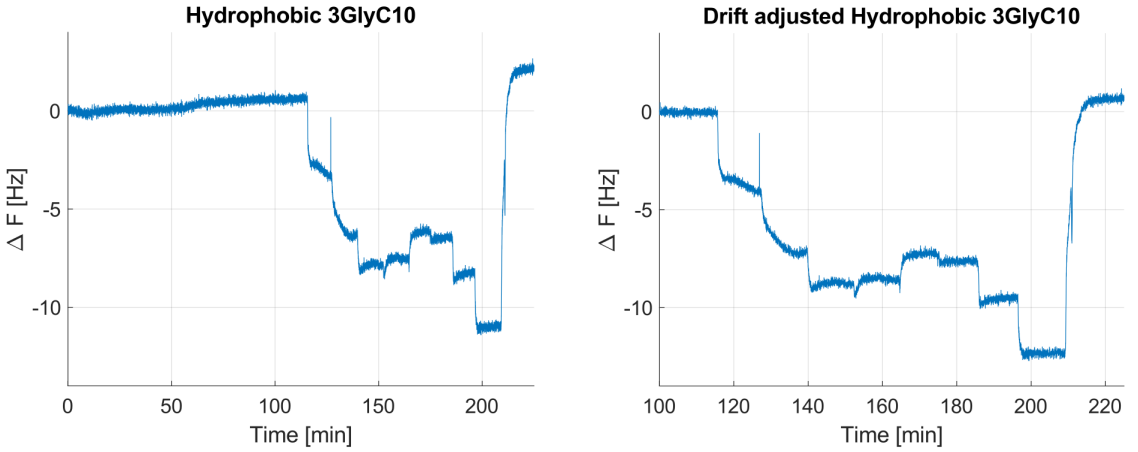

(a) Before drift adjustment.

(b) After drift adjustment.

Figure 4.12: Comparison of ΔF vs time data for triglycerol C10 ester on a hydrophobic surface, before and after adjusting for drift.

The results obtained from QCM-D measurement of the triglycerol C10 ester on a hydrophobic surface are illustrated in Figure 4.13. It can be seen that the amount of mass adsorbed onto the sensor increases for each concentration step up to 0.04%. The mass adsorption then appears to taper off and stabilize at 52 ng/cm^2, then decrease slightly for 0.013 and 0.2%, after which it again rises while the concentration increases to 1%. In Figure 4.13b, where the dissipation shift is illustrated, it can be seen that there is a slow rise and stabilization of the dissipation until 0.13%, after which the dissipation begins to rise drastically. Due to the dissipation rising significantly for 0.2-1%, the mass adsorption values obtained at these concentrations should not be considered accurate representations of the adsorbed amount due to departure from the Sauerbrey model. The last section of both plots show the measurements during the rinsing step. In both Figure 4.13a and 4.13b, the values return to approximately 0. The small difference seen is likely an effect of nonlinear shift as discussed previously.

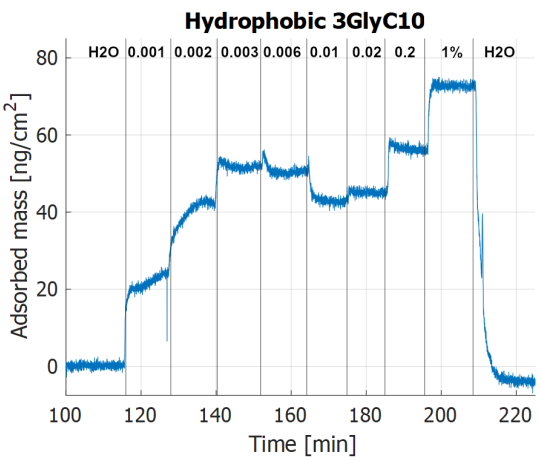

(a) Mass adsorption.

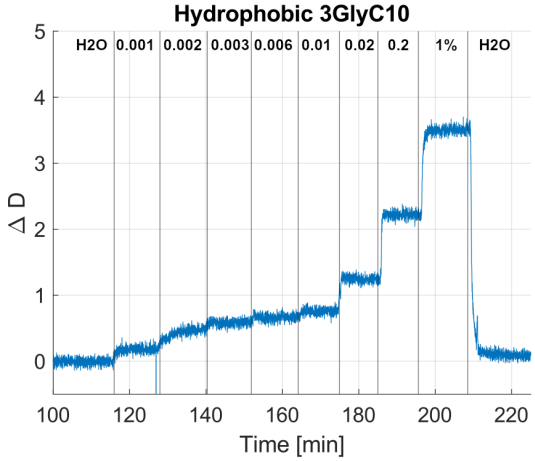

(b) Dissipation shift.

Figure 4.13: Comparison of mass adsorption and ΔD vs time data for triglycerol C10 ester on a hydrophobic surface.

The mass adsorption results obtained from the triglycerol C12 ester on a hydrophobic surface, illustrated in Figure 4.14a are mostly similar to the results obtained for the C10 ester. The mass adsorbed increases initially and stabilizes around 55 ng/cm^2 at 0.006%, after which it again starts to rise when the dissipation increases and the behavior and departs from the Sauerbrey model. The Dissipation behavior, shown in Figure 4.14b, appears to be slightly different than that obtained from the C10 ester. The dissipation initially rises slightly, but decreases below 0 after injection of the 0.006% solution and continues to decrease for the 0.01% solution. At higher concentrations 0.02%-1%, the results follow the same sharp rise seen in the C10 results. The decrease below 0 could be explained by an air bubble becoming attached to the sensor, since a dissipation shift below 0 is also seen after the water rinsing.

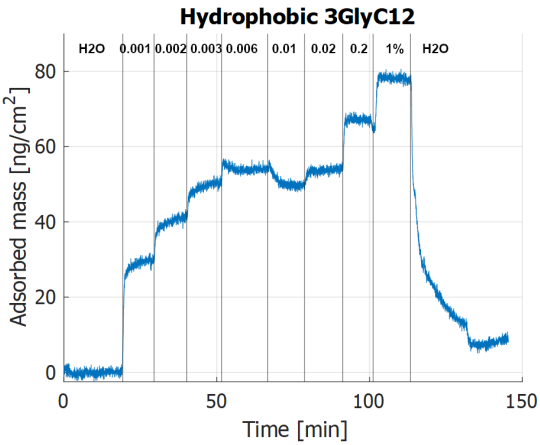

(a) Mass adsorption vs time.

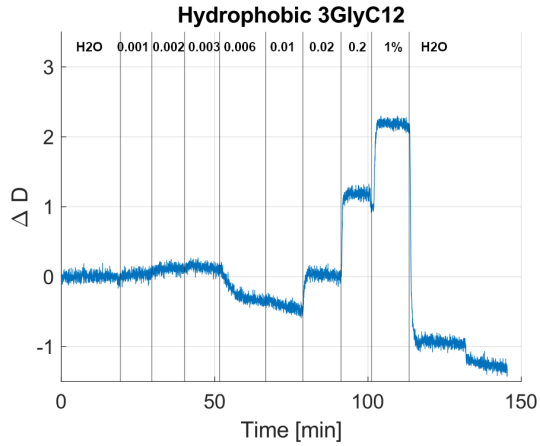

(b) Dissipation shift vs time.

Figure 4.14: Comparison of mass adsorption and ΔD vs time data for triglycerol C12 ester on a hydrophobic surface.

The adsorption behavior of the triglycerol C10 ester on hydrophilically modified surface is illustrated in Figure 4.15. It shows similar adsorption behavior as seen on the hydrophobic surface. For the first few initial concentrations below CMC, the adsorbed amount increases while the dissipation slowly rises and reaches a plateau similar to that seen in Figure 4.13b. As the dissipation starts to rise dramatically, the same trend of increased adsorbed mass with the departure from the Sauerbrey model takes place. It should be noted that the dissipation rises significantly more than what was previously seen on the hydrophobic surface, up to a maximum of 6.15 compared to 3.5. The increased adsorption during this rise in dissipation is similarly much larger than seen on the hydrophobic surface, reaching a peak value of 290 ng/cm^2. These results could be seen as indication of formation of a soft multilayered structure with high coupling to the surrounding water. Unlike the results seen from the hydrophobic surface, the rinsing does not return the adsorbed mass and dissipation shift values to anywhere close to 0. This could be seen as indication that the adsorption of the surfactant is very strong as would be expected of a strongly hydrophilic head group with the ability to hydrogen bond.

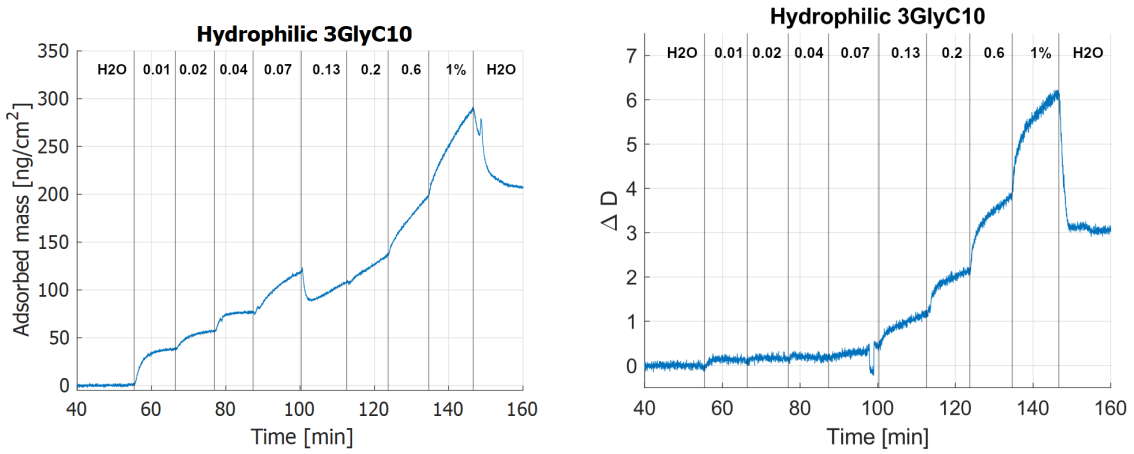

(a) Mass adsorption vs time.

(b) Dissipation shift vs time.

Figure 4.15: Comparison of mass adsorption and ΔD vs time data for triglycerol C10 ester on hydrophilically modified surface.

In an attempt to see if this was a real effect or an artifact of contamination becoming stuck to the sensor, the sensor was injected with a high flow rate of isopropanol followed by more water. As seen by the results of this procedure in Figure 4.16, the adsorbed mass moves from approximately 208 ng/cm^2 to 126 ng/cm^2 and the dissipation decreases slightly from 2.75 to 2.1. These result indicate that the adsorption of the triglycerol C10 ester to the hydrophilically modified sensor is very strong, based on the dissipation results, the adsorption likely happens in a multi layer fashion with significant amount of coupling to the surrounding water.

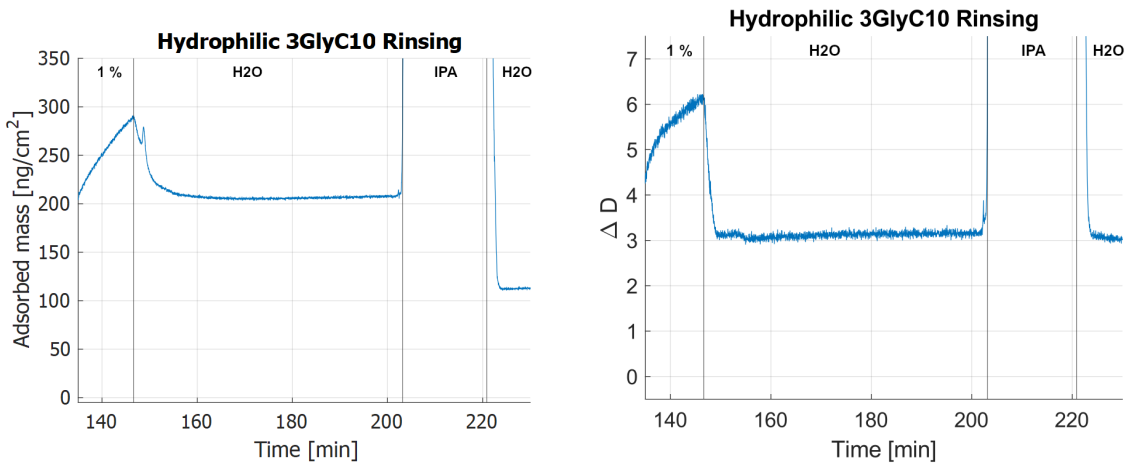

(a) Mass adsorption. **(b)** Dissipation shift.

Figure 4.16: Comparison of mass adsorption and ΔD vs time data during rinsing with water and isopropanol.

Plotting the average mass adsorption during the end of each concentration injection shows similar results for both the C10 and C12 ester on hydrophobic surfaces as seen in Figures 4.17a and 4.17b. For both the C10 and C12 ester, the adsorbed amount peaks slightly before the CMC at a little over 50 ng/cm^2, after which is then rises slightly as the concentration further increases. Comparing these results to the adsorption seen on the hydrophilically modified surface (Figure 4.17c) shows that the adsorbed amount below and up to the CMC on hydrophilic surface is approximately twice as as large as on a hydrophobic surface, around 100 ng/cm^2 compared to 50 ng/cm^2. The adsorbed amount being approximately double that on hydrophobic surface indicates the formation of a surfactant double layer. Adsorption on hydrophilic surface occurs by the polar head group interacting with the hydrophilic surface, leaving the surfactant tails pointing toward the solution phase. A second layer of surfactant can then adsorb onto the hydrophobic tail layer and forming a surfactant double layer. Further indication of double layer formation can be seen in the dissipation exhibited from the adsorbed layer on hydrophilic surface (Figure 4.15b), where the dissipation reaches a maximum value approximately twice as high as on the hydrophobic surface (Figure 4.13b).

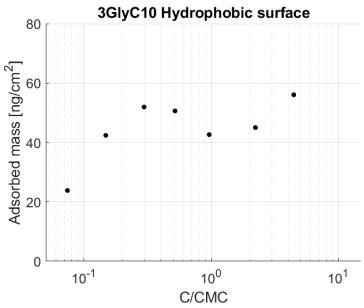

(a) 3GlyC10 on a hydrophobic surface.

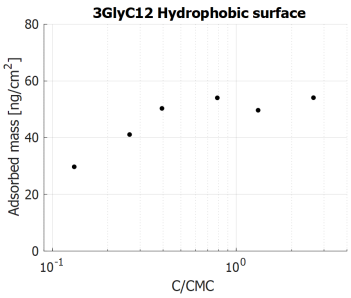

(b) 3GlyC12 on a hydrophobic surface.

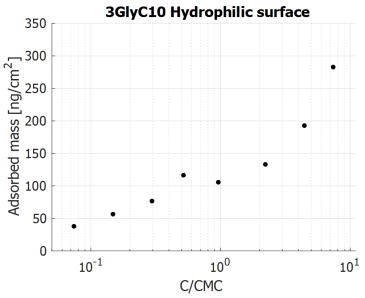

(c) 3GlyC10 on hydrophilic surface.

Figure 4.17: Mass adsorption vs C/CMC

5

Conclusion

Four different polyglycerol surfactants with varied head group branching and tail length were synthesized in this work. These consisted of three branched triglycerol esters with tail lengths of 10, 12 and 14 carbon atoms as well as one branched heptaglycerol surfactant with a tail length of 14 carbon atoms. All 4 surfactants were characterized by pendant drop tensiometry and pulsating drop interfacial rheology. Two of the triglycerol esters, C10 and C12, were also analyzed by quartz crystal microbalance with dissipation monitoring (QCM-D).

The tensiometry results showed a decrease in CMC and area per molecule with increasing tail group size for the triglycerol esters. The heptaglycerol C14 ester CMC was significantly higher than that of the triglycerol C14 ester. These results are in agreement with expectation from hydrophobic-lipophilic balance theory. The results also showed that the calculated area per molecule on the air-water interface was significantly larger for the heptaglycerol ester, this was also expected due to the substantial size of the heptaglycerol head group.

Interfacial rheology indicated that the air-water interfaces with polyglycerol surfactants exhibited significant visco-elastic character when the concentration was close to the CMC, indicating the presence of strong intermolecular interactions between the surfactant molecules. The effect of the tail length was difficult to discern from the acquired data, indicating that the head group is likely responsible for the observed effect. Increase in the size of the branched head group seemed resulted in further increase in interface visco-elasticity, likely due to the heptaglycerol head group featuring a larger structure with more polar groups available for interaction.

QCM-D analysis on hydrophobic surface did not show significant difference with increased tail length. Analysis on hydrophilic surface showed significantly stronger adsorption as compared to on hydrophobic due to the stronger polar interactions and possible hydrogen bonding. High dissipation values on hydrophilic surface indicated that the adsorbed surfactant structure is strongly coupled to the liquid medium, possibly due to the formation of a surfactant double layer. The formation of a surfactant double layer was additionally supported by the adsorbed mass being approximately twice as large on the hydrophilic surface as compared to hydrophobic.

In order to further investigate and clarify the structure-property relationship in polyglycerol surfactants it would be prudent to directly compare branched polyglycerol structures with linear structures containing an equal number of glycerol units.

Based on the strong adsorption seen on hydrophilically modified surface it would also be of interest to compare the behavior of branched structures with linear structures in order to clarify what effect the structure of the head group plays. It may also be of interest to compare branched polyglycerol surfactants with polyethylene oxide surfactants by interfacial rheology in order to investigate what role the hydroxyl groups have in intermolecular interactions on the air-water interface.

6

References

[1] J.L Salager. *Surfactants types and uses*. FIRP Booklet, 2002.

[2] Abhyarthana Pattanaik and Rayasam Venugopal. "Role of Surfactants in Mineral Processing: An Overview". In: *Surfactants and Detergents*. IntechOpen, Nov. 2019. ISBN: 9781789846614. DOI: 10.5772/intechopen.85947. URL: http://dx.doi.org/10.5772/intechopen.85947.

[3] Rudy Thomas P and West Jack K. *Surfactant additives for solid propellants*. US Patent US4221617A, September. 1966.

[4] Bengt Kronberg, Krister Holmberg, and Björn Lindman. *Surface Chemistry of Surfactants and Polymers*. Wiley, Sept. 2014. ISBN: 9781118695968. DOI: 10.1002/9781118695968. URL: http://dx.doi.org/10.1002/9781118695968.

[5] R. G. Alargova et al. "Micelle Aggregation Numbers of Surfactants in Aqueous Solutions: A Comparison between the Results from Steady-State and Time-Resolved Fluorescence Quenching". In: *Langmuir* 14.19 (Aug. 1998), pp. 5412–5418. ISSN: 1520-5827. DOI: 10.1021/la980565x. URL: http://dx.doi.org/10.1021/la980565x.

[6] D. C. Cullum. "Surfactant types; classification, identification, separation". In: *Introduction to Surfactant Analysis*. Ed. by D. C. Cullum. Dordrecht: Springer Netherlands, 1994, pp. 17–41. ISBN: 978-94-011-1316-8. DOI: 10.1007/978-94-011-1316-8_2. URL: https://doi.org/10.1007/978-94-011-1316-8_2.

[7] Suruchi Damle and Chandu Madankar. "An overview on eco-friendly polyglycerol esters of fatty acid, synthesis and applications". In: *Tenside Surfactants Detergents* 60.6 (Oct. 2023), pp. 611–621. ISSN: 2195-8564. DOI: 10.1515/tsd-2023-2509. URL: http://dx.doi.org/10.1515/tsd-2023-2509.

[8] Anja Thomas, Sophie S. Müller, and Holger Frey. "Beyond Poly(ethylene glycol): Linear Polyglycerol as a Multifunctional Polyether for Biomedical and Pharmaceutical Applications". In: *Biomacromolecules* 15.6 (May 2014), pp. 1935–1954. ISSN: 1526-4602. DOI: 10.1021/bm5002608. URL: http://dx.doi.org/10.1021/bm5002608.

[9] Achille Antenucci et al. "Design, Synthesis and Application of C2-Symmetric Cycloglycerodiphosphate Catalysts". In: *Advanced Synthesis amp; Catalysis* 365.8 (Apr. 2023), pp. 1170–1178. ISSN: 1615-4169. DOI: 10.1002/adsc.202300136. URL: http://dx.doi.org/10.1002/adsc.202300136.

[10] Ryan Gilmour and Christoph Bucher. "A Modular Synthesis of Fluorinated, Chiral Polar Lipids". In: *Synthesis* 2011.04 (Jan. 2011), pp. 549–552. ISSN: 1437-210X. DOI: 10.1055/s-0030-1258413. URL: http://dx.doi.org/10.1055/s-0030-1258413.

[11] Daniel, Wayne, and Lemke. *Surfactant additives for solid propellants*. US Patent US6620904B2, November. 2001.

[12] Negisa Ebadipour et al. "Alkaline-Based Catalysts for Glycerol Polymerization Reaction: A Review". In: *Catalysts* 10.9 (Sept. 2020), p. 1021. ISSN: 2073-4344. DOI: 10.3390/catal10091021. URL: http://dx.doi.org/10.3390/catal10091021.

[13] Gabor A Somorjai. *Introduction to surface chemistry and catalysis*. en. Ed. by Gabor A Somorjai. Nashville, TN: John Wiley & Sons, Apr. 1994.

[14] M V Berry. "The molecular mechanism of surface tension". In: *Physics Education* 6.2 (Mar. 1971), pp. 79–84. ISSN: 0031-9120. DOI: 10.1088/0031-9120/6/2/001. URL: http://dx.doi.org/10.1088/0031-9120/6/2/001.

[15] Svein Skjæveland. *Derivations of the Young-Laplace equation*. Nov. 2015. DOI: 10.13140/RG.2.1.4485.5768.

[16] Clyde E. Stauffer. "The Measurement of Surface Tension by the Pendant Drop Technique". In: *The Journal of Physical Chemistry* 69.6 (June 1965), pp. 1933–1938. ISSN: 1541-5740. DOI: 10.1021/j100890a024. URL: http://dx.doi.org/10.1021/j100890a024.

[17] Joseph D. Berry et al. "Measurement of surface and interfacial tension using pendant drop tensiometry". In: *Journal of Colloid and Interface Science* 454 (Sept. 2015), pp. 226–237. ISSN: 0021-9797. DOI: 10.1016/j.jcis.2015.05.012. URL: http://dx.doi.org/10.1016/j.jcis.2015.05.012.

[18] Reinhard Miller and Libero Liggieri, eds. *Interfacial rheology*. en. Progress in Colloid and Interface Science. London, England: CRC Press, Dec. 2019.

[19] Reinhard Miller et al. "Rheology of interfacial layers". In: *Colloid and Polymer Science* 288.9 (May 2010), pp. 937–950. ISSN: 1435-1536. DOI: 10.1007/s00396-010-2227-5. URL: http://dx.doi.org/10.1007/s00396-010-2227-5.

[20] José M. Zamora et al. "Interfacial rheology of low interfacial tension systems using a new oscillating spinning drop method". In: *Journal of Colloid and Interface Science* 519 (June 2018), pp. 27–37. ISSN: 0021-9797. DOI: 10.1016/j.jcis.2018.02.015. URL: http://dx.doi.org/10.1016/j.jcis.2018.02.015.

[21] Nimibofa Ayawei, Augustus Newton Ebelegi, and Donbebe Wankasi. "Modelling and Interpretation of Adsorption Isotherms". In: *Journal of Chemistry* 2017 (2017), pp. 1–11. ISSN: 2090-9071. DOI: 10.1155/2017/3039817. URL: http://dx.doi.org/10.1155/2017/3039817.

[22] N. Sivarajasekar and R. Baskar. "Adsorption of basic red 9 onto activated carbon derived from immature cotton seeds: isotherm studies and error analysis". In: *Desalination and Water Treatment* 52.40–42 (Sept. 2013), pp. 7743–7765. ISSN: 1944-3986. DOI: 10.1080/19443994.2013.834518. URL: http://dx.doi.org/10.1080/19443994.2013.834518.

[23] Hans Swenson and Nicholas P. Stadie. "Langmuir's Theory of Adsorption: A Centennial Review". In: *Langmuir* 35.16 (Mar. 2019), pp. 5409–5426. ISSN: 1520-5827. DOI: 10.1021/acs.langmuir.9b00154. URL: http://dx.doi.org/10.1021/acs.langmuir.9b00154.

[24] Shams Kalam et al. "Surfactant Adsorption Isotherms: A Review". In: *ACS Omega* 6.48 (Nov. 2021), pp. 32342–32348. ISSN: 2470-1343. DOI: 10.1021/acsomega.1c04661. URL: http://dx.doi.org/10.1021/acsomega.1c04661.

[25] Guangming Liu and Guangzhao Zhang. *QCM-D Studies on Polymer Behavior at Interfaces*. Springer Berlin Heidelberg, 2013. ISBN: 9783642397905. DOI: 10.1007/978-3-642-39790-5. URL: http://dx.doi.org/10.1007/978-3-642-39790-5.

[26] Ralf P. Richter et al. "Coupling Spectroscopic Ellipsometry and Quartz Crystal Microbalance to Study Organic Films at the Solid–Liquid Interface". In: *Springer Series in Surface Sciences*. Springer International Publishing, 2018, pp. 391–417. ISBN: 9783319758954. DOI: 10.1007/978-3-319-75895-4_17. URL: http://dx.doi.org/10.1007/978-3-319-75895-4_17.

[27] Gunnar Dunér, Esben Thormann, and Andra Dėdinaitė. "Quartz Crystal Microbalance with Dissipation (QCM-D) studies of the viscoelastic response from a continuously growing grafted polyelectrolyte layer". In: *Journal of Colloid and Interface Science* 408 (Oct. 2013), pp. 229–234. ISSN: 0021-9797. DOI: 10.1016/j.jcis.2013.07.008. URL: http://dx.doi.org/10.1016/j.jcis.2013.07.008.

[28] James M. Bell et al. "Acetal Formation for Ketones and Aromatic Aldehydes with Methanol1". In: *The Journal of Organic Chemistry* 30.12 (Dec. 1965), pp. 4284–4292. ISSN: 1520-6904. DOI: 10.1021/jo01023a067. URL: http://dx.doi.org/10.1021/jo01023a067.

[29] Jonathan Clayden, Nick Greeves, and Stuart Warren. *Organic Chemistry*. 2nd ed. London, England: Oxford University Press, Mar. 2012.

[30] Alejandro Leal-Duaso et al. "Glycerol-Derived Solvents: Synthesis and Properties of Symmetric Glyceryl Diethers". In: *ACS Sustainable Chemistry & Engineering* 7.15 (July 2019), pp. 13004–13014. ISSN: 2168-0485. DOI: 10.1021/acssuschemeng.9b02105. URL: http://dx.doi.org/10.1021/acssuschemeng.9b02105.

[31] Zerong Wang. *Comprehensive Organic Name Reactions and Reagents*. Sept. 2010. DOI: 10.1002/9780470638859. URL: http://dx.doi.org/10.1002/9780470638859.

[32] Kenji Mori. "Pheromone synthesis. Part 253: Synthesis of the racemates and enantiomers of triglycerides of male Drosophila fruit flies with special emphasis on the preparation of enantiomerically pure 1-monoglycerides". In: *Tetrahedron* 68.40 (Oct. 2012), pp. 8441–8449. ISSN: 0040-4020. DOI: 10.1016/j.tet.2012.07.086. URL: http://dx.doi.org/10.1016/j.tet.2012.07.086.

[33] Yao Xu et al. "Intramolecular Chirality Transfer [2 + 2] Cycloadditions of Allenoates and Alkenes". In: *Organic Letters* 19.14 (July 2017), pp. 3703–3706. ISSN: 1523-7052. DOI: 10.1021/acs.orglett.7b01420. URL: http://dx.doi.org/10.1021/acs.orglett.7b01420.

[34] Alain Krief and Alexandre Froidbise. "Hemisynthesis of methyl pyrethroates from -alkoxy-alkylidene malonates and isopropylidenediphenylsulfurane and isopropylidenetriphenylphosphorane". In: *Tetrahedron* 60.35 (Aug. 2004), pp. 7637–7658. ISSN: 0040-4020. DOI: 10.1016/j.tet.2004.06.035. URL: http://dx.doi.org/10.1016/j.tet.2004.06.035.

[35] Takanori Kotera and Akira Saito. *NOVEL ETHER COMPOUND*. EU Patent EP2165996B1, August. 2013.

[36] Michael Heartlein. *POLYANIONIC DELIVERY OF NUCLEIC ACIDS*. EU Patent WO2018165257A1, March. 2018.

[37] Jean-Pierre Berkan Lindner. *Coated silicon surfaces, their manufacture and application*. EU Patent EP3067381A1, September. 2016.

[38] Noriyuki Nakajima et al. "Synthesis of Cyclic Polyglycerols". In: *HETEROCYCLES* 69.1 (2006), p. 107. ISSN: 0385-5414. DOI: 10.3987/com-06-s(o)44. URL: http://dx.doi.org/10.3987/COM-06-S(O)44.

[39] Ariane Tschiche et al. "Polyglycerol-based amphiphilic dendrons as potential siRNA carriers for in vivo applications". In: *J. Mater. Chem. B* 2.15 (2014), pp. 2153–2167. ISSN: 2050-7518. DOI: 10.1039/c3tb21364a. URL: http://dx.doi.org/10.1039/c3tb21364a.

[40] Monika Wyszogrodzka and Rainer Haag. "A Convergent Approach to Biocompatible Polyglycerol "Click" Dendrons for the Synthesis of Modular Core–Shell Architectures and Their Transport Behavior". In: *Chemistry – A European Journal* 14.30 (Oct. 2008), pp. 9202–9214. ISSN: 1521-3765. DOI: 10.1002/chem.200800892. URL: http://dx.doi.org/10.1002/chem.200800892.

[41] Louise F. Walker et al. "Synthesis of 2, 5-dihydrofurans via alkylidene carbene insertion reactions". In: *Journal of the Chemical Society, Perkin Transactions 1* 7 (Feb. 2002), pp. 965–981. ISSN: 1364-5463. DOI: 10.1039/b111097g. URL: http://dx.doi.org/10.1039/b111097g.

[42] E. Del Rio et al. "Polyurethanes from polyols obtained by ADMET polymerization of a castor oil-based diene: Characterization and shape memory properties". In: *Journal of Polymer Science Part A: Polymer Chemistry* 49.2 (Nov. 2010), pp. 518–525. ISSN: 1099-0518. DOI: 10.1002/pola.24466. URL: http://dx.doi.org/10.1002/pola.24466.

[43] Otto; Petrus Philippus and Hermann; Leonardus. *75 Se and 123m Te Compounds for fat resorption tests*. US Patent US3993741A, November. 1976.

[44] Haopeng Wang et al. “Sequentially Adsorbed Electrostatic Multilayers of Branched Side-Chain Polyelectrolytes Bearing DonorAcceptor Type Azo Chromophores”. In: *Macromolecules* 37.1 (Dec. 2003), pp. 135–146. ISSN: 1520-5835. DOI: 10.1021/ma035208u. URL: http://dx.doi.org/10.1021/ma035208u.

[45] Heinz Günter Viehe, Brigitte Le Clef, and Asher Elgavi. “Reactions of Acyl Chlorides/Triethylamine or Ketenes with Phosgeniminium Salts”. In: *Angewandte Chemie International Edition in English* 16.3 (Mar. 1977), pp. 182–182. ISSN: 0570-0833. DOI: 10.1002/anie.197701821. URL: http://dx.doi.org/10.1002/anie.197701821.

[46] Piers R. J. Gaffney and Colin B. Reese. “Synthesis of naturally occurring phosphatidylinositol 3,4,5-trisphosphate [PtdIns(3,4,5)P3] and its diastereoisomers”. In: *Journal of the Chemical Society, Perkin Transactions 1* 2 (2001), pp. 192–205. ISSN: 1364-5463. DOI: 10.1039/b007267m. URL: http://dx.doi.org/10.1039/B007267M.

[47] Wei Li et al. “Mechanistic Pathways in CF3COOH-Mediated Deacetalization Reactions”. In: *The Journal of Organic Chemistry* 75.4 (Jan. 2010), pp. 1077–1086. ISSN: 1520-6904. DOI: 10.1021/jo902014z. URL: http://dx.doi.org/10.1021/jo902014z.

7
Appendix

Obtained FTIR, NMR, MSMS and QCM-D data discussed in this work are included in this section.

7.1 Solketal

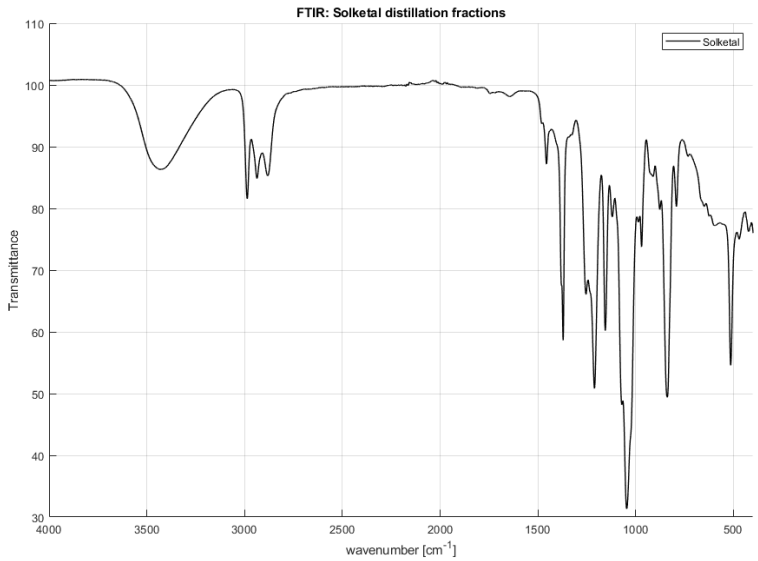

Figure 7.1: FTIR spectrum of distilled solketal.

FTIR (neat): v 3433 (OH), 2986, 2939, 2881, 1456, 1371, 1256, 1211, 1155, 1120, 1070, 1046, 985, 969, 911, 877, 839, 792, 731, 651, 625, 592, 515, 471, 421 cm^{-1}.

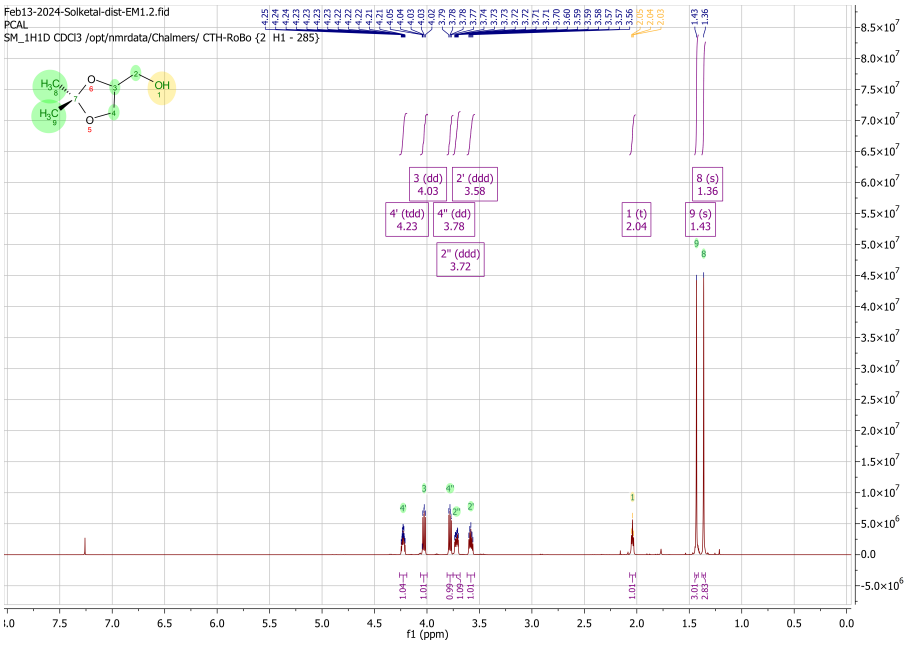

Figure 7.2: ^{1}H NMR spectrum of distilled solketal in $CDCl_3$.

1H NMR (600 MHz, CDCl3) δ 4.23 (tdd, J = 6.5, 5.2, 3.7 Hz, 1H), 4.03 (dd, J = 8.2, 6.6 Hz, 1H), 3.78 (dd, J = 8.2, 6.5 Hz, 1H), 3.72 (ddd, J = 11.6, 5.7, 3.7 Hz, 1H), 3.58 (ddd, J = 11.6, 6.5, 5.2 Hz, 1H), 2.04 (t, J = 6.2 Hz, 1H), 1.43 (s, 3H), 1.36 (s, 3H).

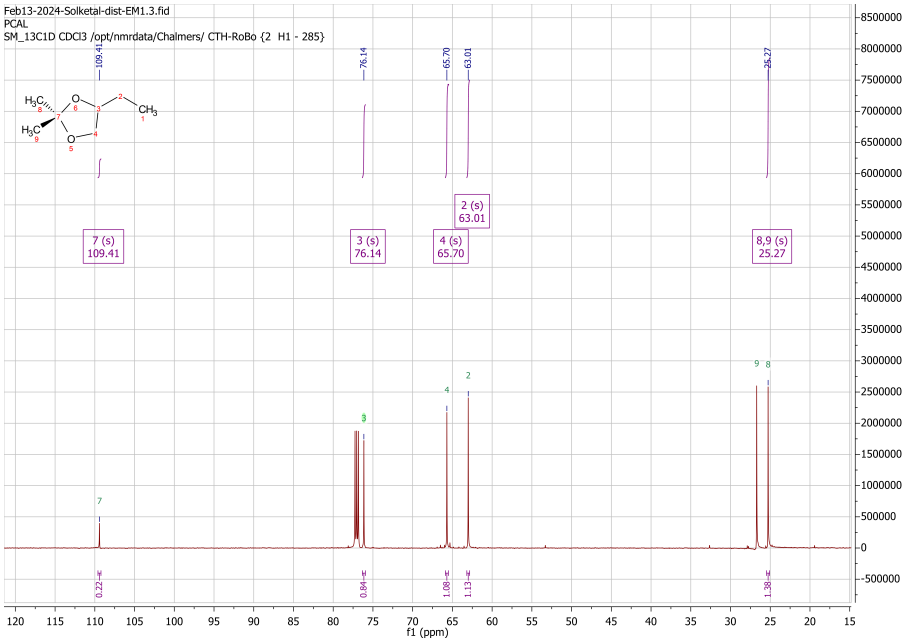

Figure 7.3: ^{13}C NMR spectrum of distilled solketal in $CDCl_3$.

13C NMR (151 MHz, $CDCl_3$) δ 109.41, 76.14, 65.70, 63.01, 25.27.

7.2 Triglycerol ketal

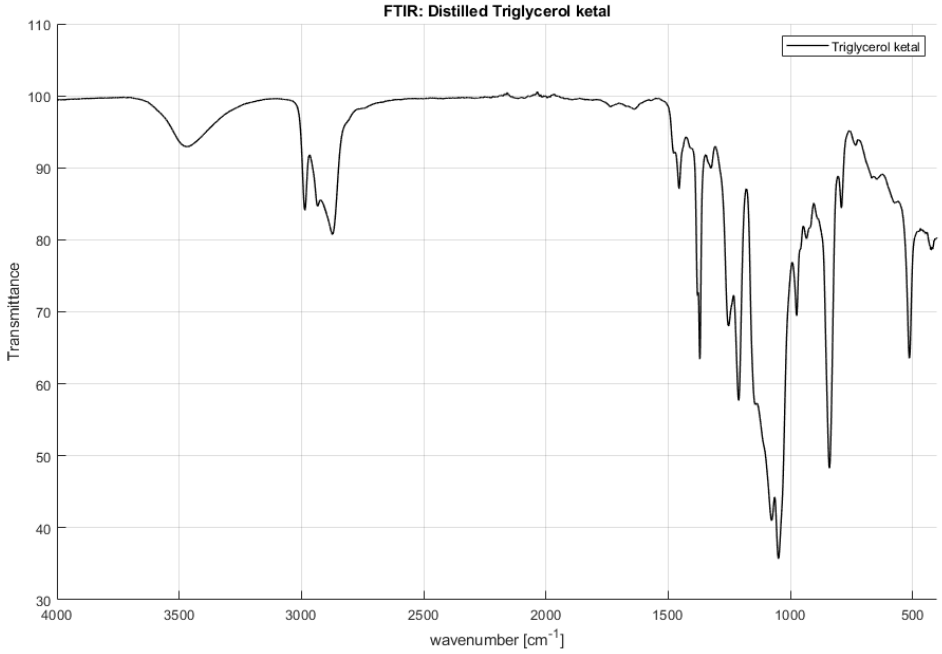

Figure 7.4: FTIR spectrum of distilled triglycerol ketal.

FTIR (neat): v 3471 (OH),2986, 2936, 2871, 1479, 1456, 1380, 1371, 1325, 1253, 1212, 1144, 1078, 1049, 975, 935, 841, 733, 668, 647, 573, 514, 426 cm^{-1}.

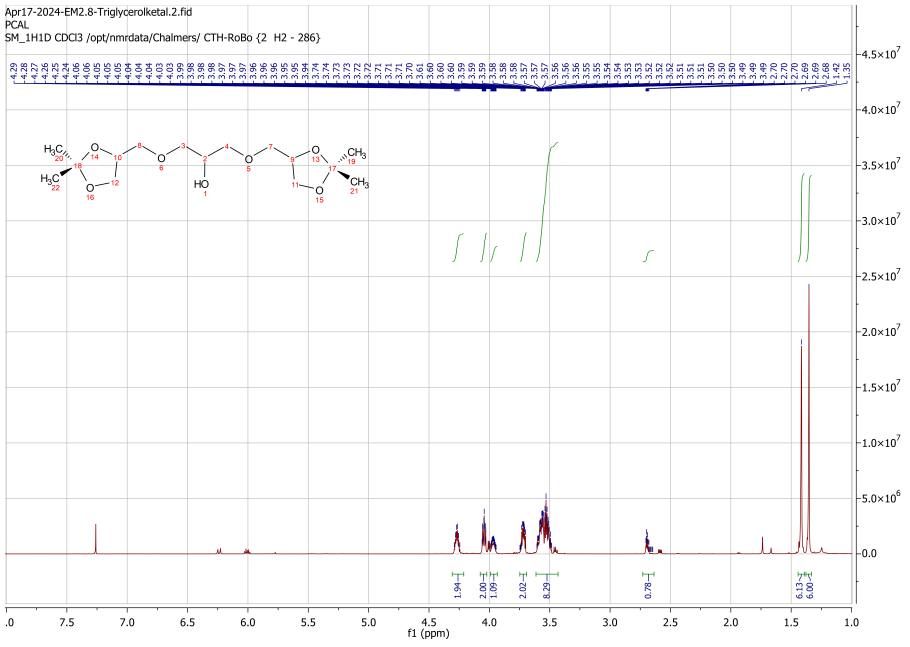

Figure 7.5: ^{1}H NMR spectrum of distilled triglycerol ketal in $CDCl_3$.

1H NMR (600 MHz, $CDCl_3$) δ 4.27 (dq, J = 11.9, 6.1 Hz, 2H), 4.04 (ddt, J = 8.1, 6.5, 1.9 Hz, 2H), 3.96 (ttt, J = 8.8, 4.2, 2.0 Hz, 1H), 3.75 – 3.69 (m, 2H), 3.55 (dtddd, J = 71.9, 18.7, 16.9, 13.0, 7.2, 4.2 Hz, 8H), 2.73-2.64 (dt, J = 2.69, 1 H) ii, 1.42 (s, 6H), 1.35 (s, 6H).

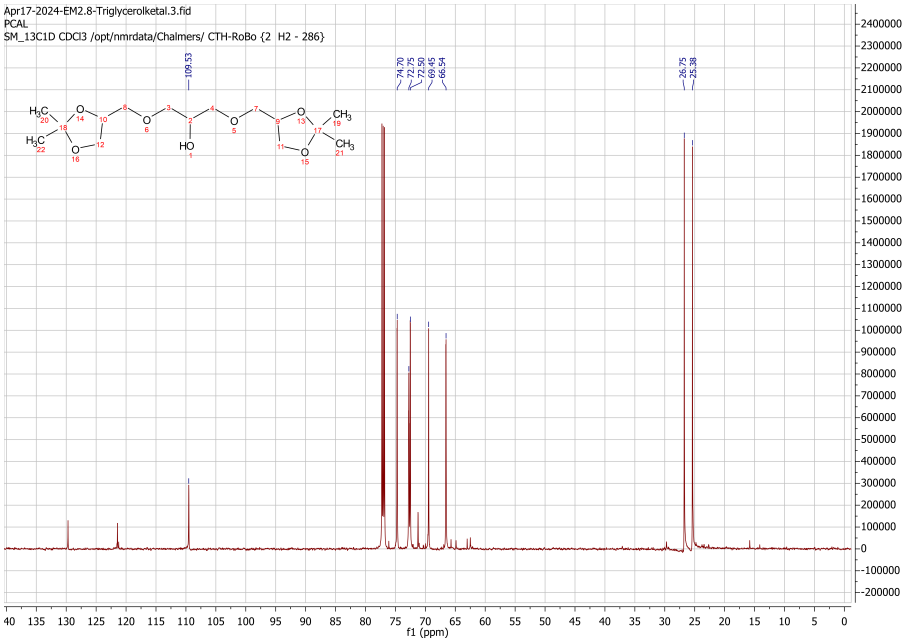

Figure 7.6: ^{13}C NMR spectrum of distilled triglycerol ketal in $CDCl_3$.

13C NMR (151 MHz, $CDCl_3$) δ 109.53, 74.70, 72.75, 72.50, 69.45, 66.54, 26.75, 25.38.

7.3 Esterification and deprotection of triglycerol ketal

7.3.1 Triglycerol ketal C12 ester

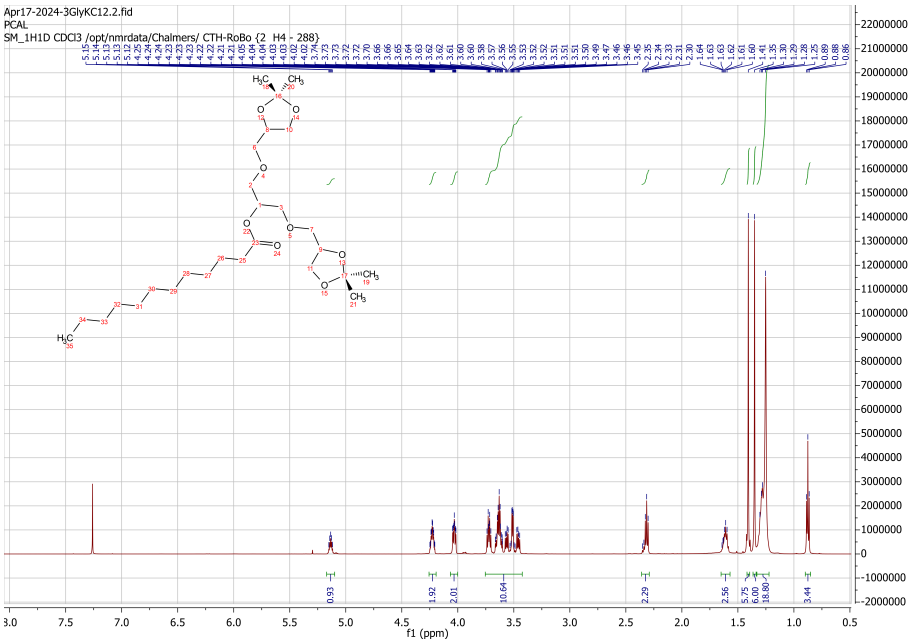

Figure 7.7: ^{1}H NMR spectrum of triglycerol ketal C12 ester in $CDCl_3$.

^{1}H NMR (600 MHz, $CDCl_3$) δ 5.17-5.10f (hept, 1H), 4.26-4.19 (pd, 2H), 4.06-4.00 (ddd, 2H), 3.75 – 3.42 (m, 11H), 2.36-2.29 (t, 2H), 1.65-1.57 (q, 3H), 1.42-1.39 (s, 6H), 1.36-1.34 (s, 6H), 1.33-1.22 (d, 19H), 0.9-0.85 (t, 3H).

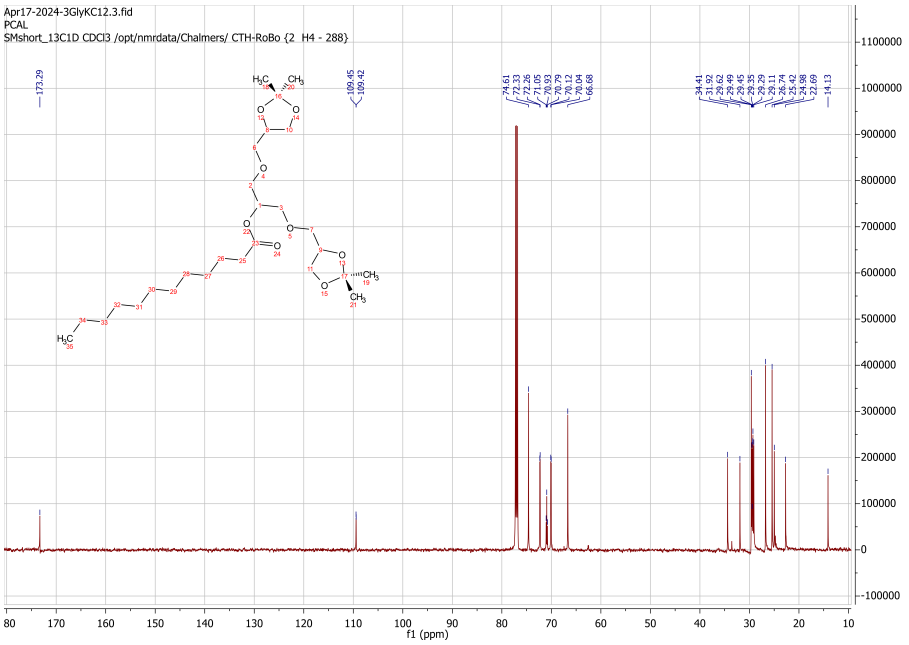

Figure 7.8: ^{13}C NMR spectrum of triglycerol ketal C12 ester in $CDCl_3$.

^{13}C NMR (151 MHz, $CDCl_3$) δ 173.29, 109.45, 109.42, 74.61, 72.33, 72.26, 71.05, 70.93, 70.79, 70.12, 70.04, 66.68, 34.41, 31.92, 29.62, 29.49, 29.45, 29.35, 29.29, 29.11, 26.74, 25.42, 24.98, 22.69, 14.13.

7.3.2 Triglycerol ketal C14 ester

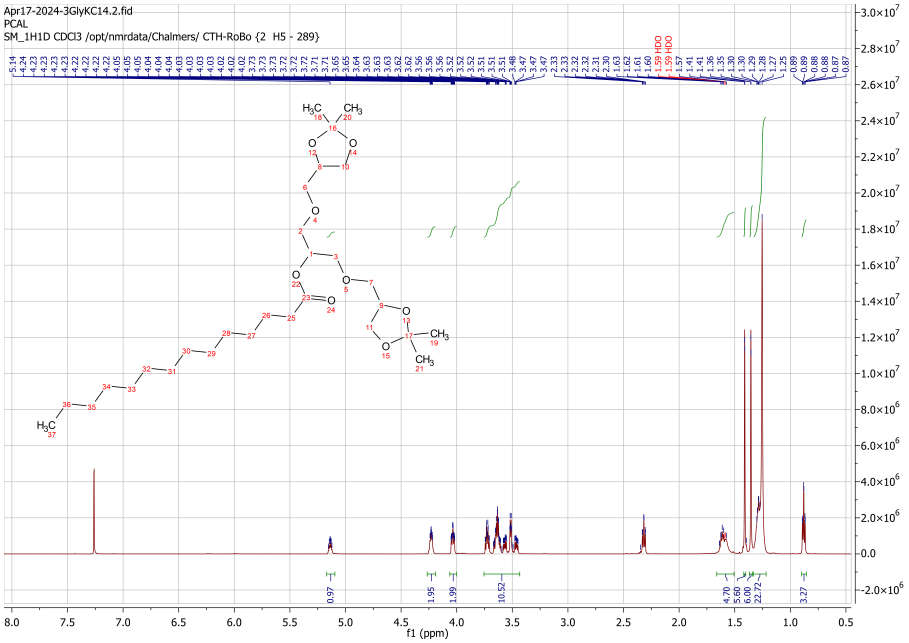

Figure 7.9: ^{1}H NMR spectrum of triglycerol ketal C14 ester in $CDCl_3$.

^{1}H NMR (600 MHz, $CDCl_3$) δ 5.17-5.09 (dtd, 1H), 4.26 – 4.19 (m, 2H), 4.06-4.00 (dddd, 2H), 3.76 – 3.43 (m, 11H), 2.36-2.29 (td, 2Hz), 1.66 – 1.51 (m, 5H), 1.42-1.40 (s, 6H), 1.37-1.34 (s, 6H), 1.33-1.22 (m, 23H), 0.90-0.86 (td, 3H).

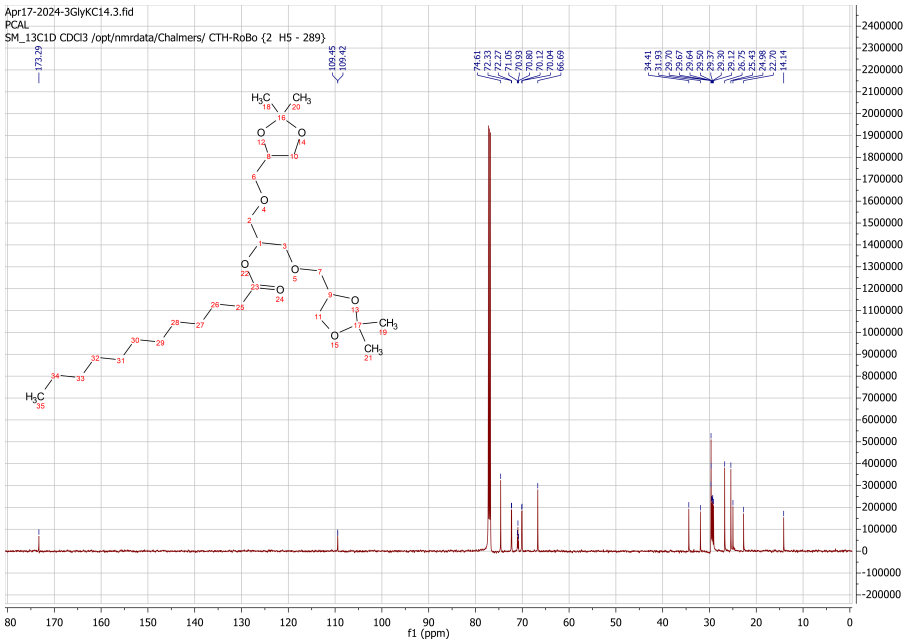

Figure 7.10: ^{13}C NMR spectrum of triglycerol ketal C14 ester in $CDCl_3$.

^{13}C NMR (151 MHz, $CDCl_3$) δ 173.29, 109.45, 109.42, 74.61, 72.33, 72.27, 71.05, 70.93, 70.80, 70.12, 70.04, 66.69, 34.41, 31.93, 29.70, 29.67, 29.64, 29.50, 29.37, 29.30, 29.12, 26.75, 25.43, 24.98, 22.70, 14.14.

7.3.3 Triglycerol C10 ester

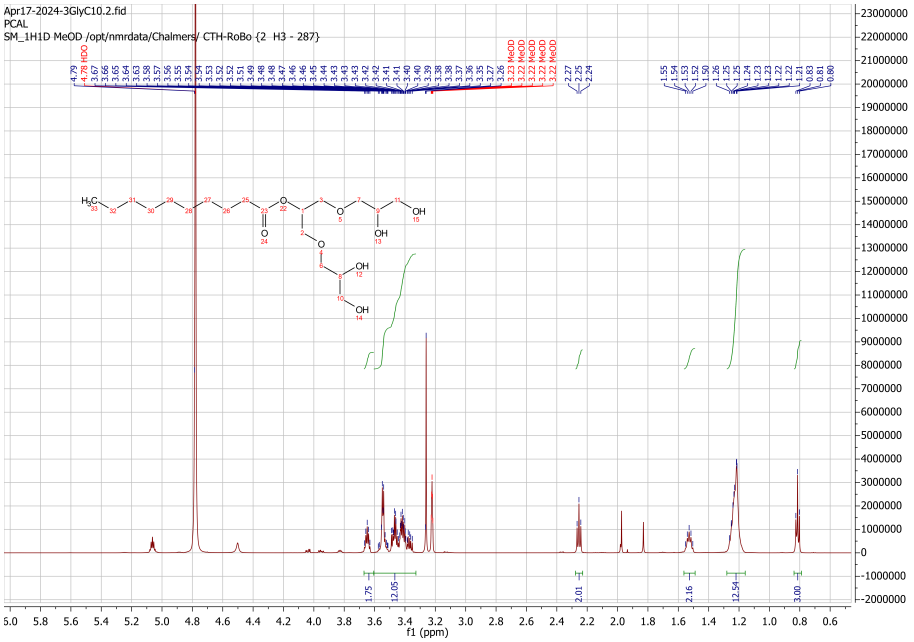

Figure 7.11: ^{1}H NMR spectrum of triglycerol C10 ester in MeOD.

^{1}H NMR (600 MHz, MeOD) δ 3.67-3.61 (p, 2H), 3.61-3.33 (m, 12H), 2.28-2.23 (t, 2H), 1.56-1.49 (p, 2H), 1.28–1.16 (m, 13H), 0.84-0.79 (t, 3H).

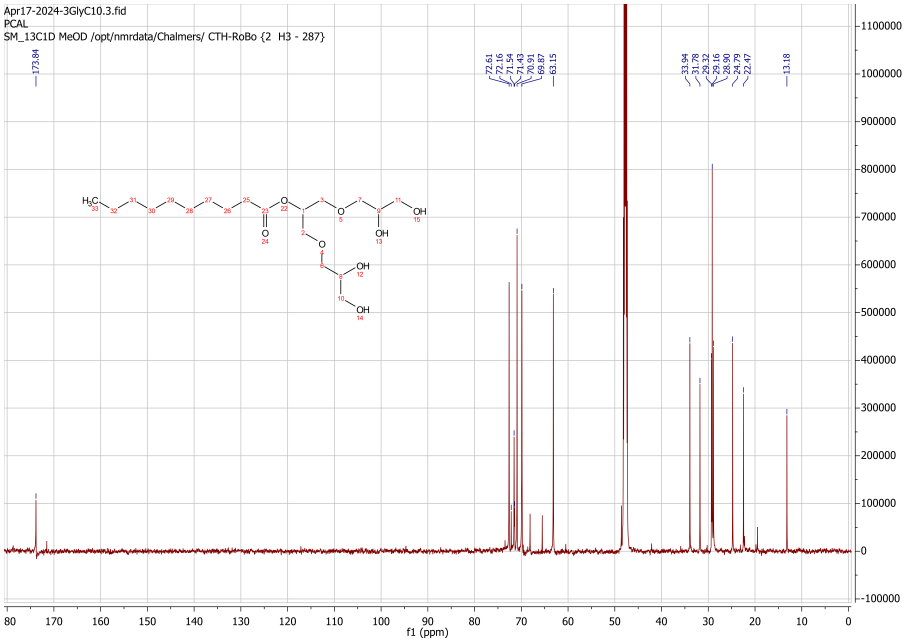

Figure 7.12: ^{13}C NMR spectrum of triglycerol C10 ester in MeOD.

^{13}C NMR (151 MHz, MeOD) δ 173.84, 72.61, 72.16, 71.54, 71.43, 70.91, 69.87, 63.15, 33.94, 31.78, 29.32, 29.16, 28.90, 24.79, 22.47, 13.18.

7.3.4 Triglycerol C12 ester

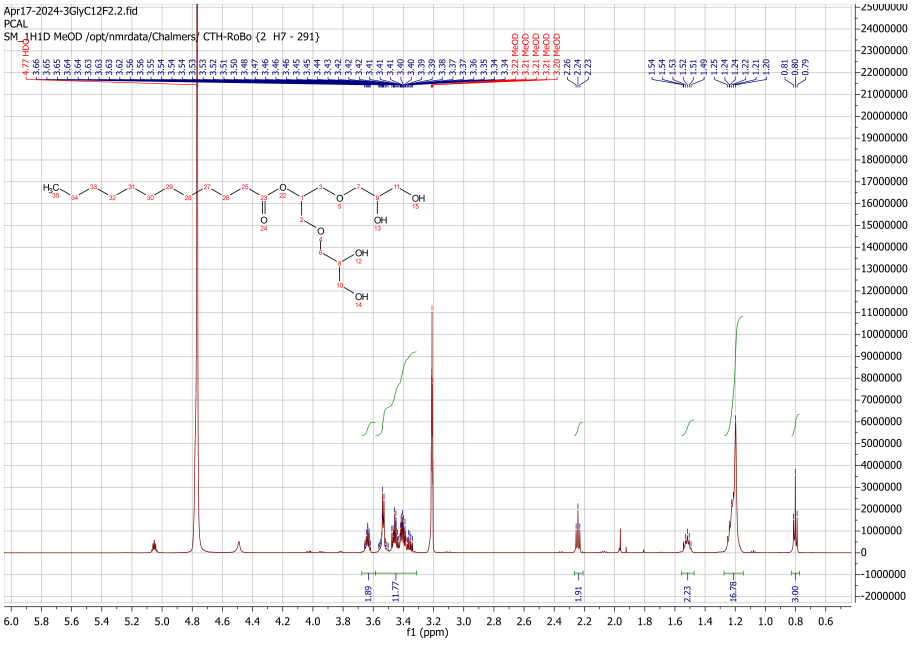

Figure 7.13: ^{1}H NMR spectrum of triglycerol C12 ester in MeOD.

^{1}H NMR (600 MHz, MeOD) δ 3.68–3.59 (m, 2H), 3.59–3.31 (m, 12H), 2.27-2.20 (t, 2H), 1.56-1.47 (p, 2H), 1.27-1.14 (d, 17H), 0.82-0.77 (t, 3H).

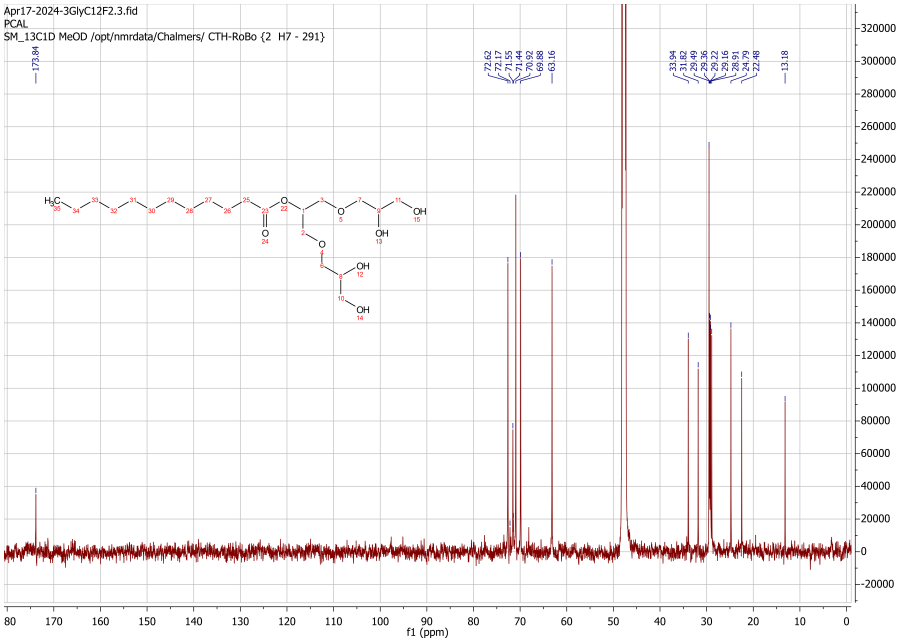

Figure 7.14: ^{13}C NMR spectrum of triglycerol C12 ester in MeOD.

^{13}C NMR (151 MHz, MeOD) δ 173.84, 72.62, 72.17, 71.55, 71.44, 70.92, 69.88, 63.16, 33.94, 31.82, 29.49, 29.36, 29.22, 29.16, 28.91, 24.79, 22.48, 13.18.

7.3.5 Triglycerol C14 ester

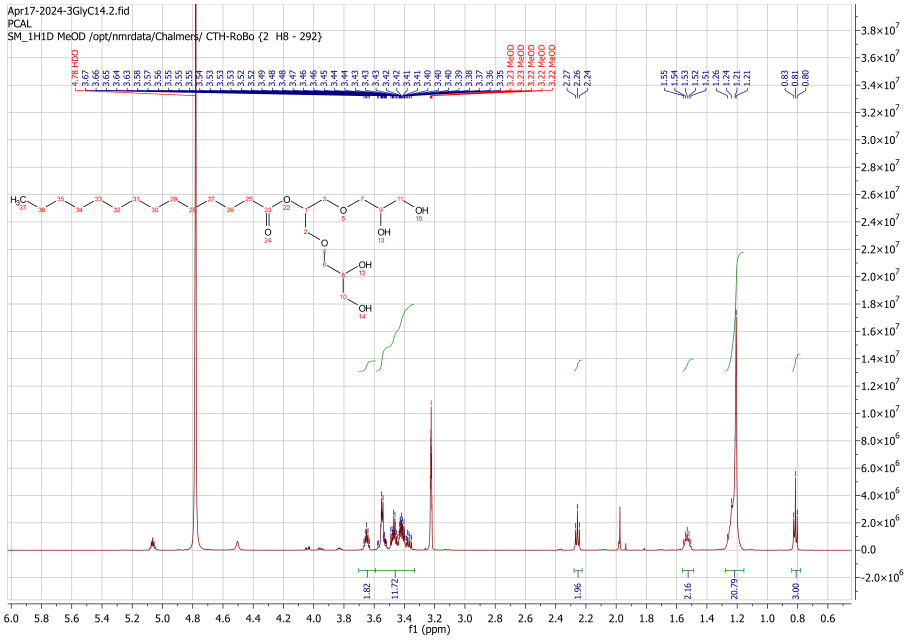

Figure 7.15: ^{1}H NMR spectrum of triglycerol C14 ester in MeOD.

^{1}H NMR (600 MHz, MeOD) δ 3.70-3.59 (p, 2H), 3.59–3.33 (m, 12H), 2.28-2.22 (t, 2H), 1.57-1.47 (t, 2H), 1.28-1.15 (d, 21H), 0.84-0.78 (t, 3H).

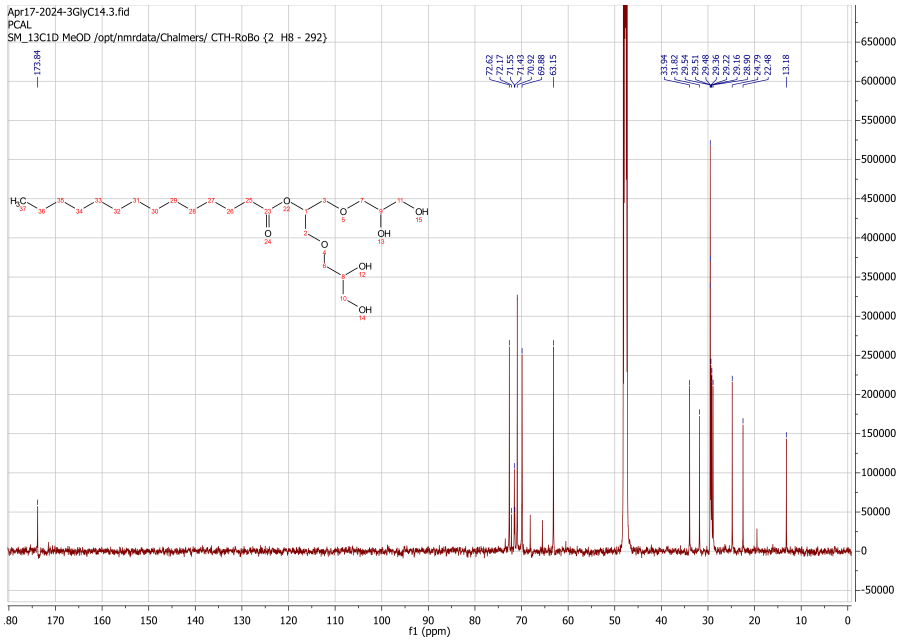

Figure 7.16: ^{13}C NMR spectrum of triglycerol C14 ester in MeOD.

^{13}C NMR (151 MHz, MeOD) δ 173.84, 72.62, 72.17, 71.55, 71.43, 70.92, 69.88, 63.15, 33.94, 31.82, 29.54, 29.51, 29.48, 29.36, 29.22, 29.16, 28.90, 24.79, 22.48, 13.18.

7.4 Heptaglycerol ketal

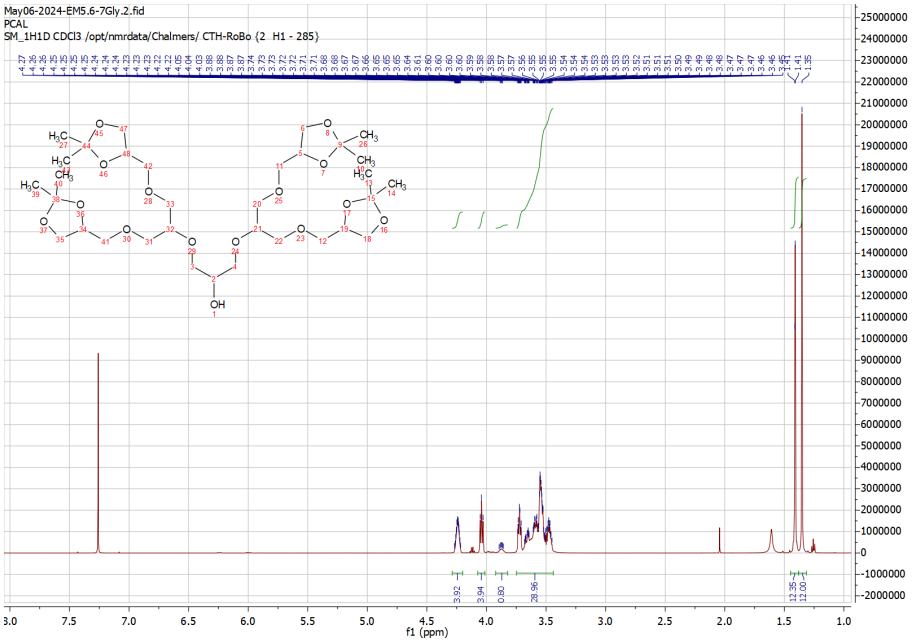

Figure 7.17: ^{1}H NMR spectrum of heptaglycerol ketal in $CDCl_3$.

^{1}H NMR (600 MHz, $CDCl_3$) δ 4.29-4.2 (m, 4H), 4.07-4.01 (t, 4H), 3.92-3.82 (m, 1H), 3.75-3.44 (m, 29H), 1.45-1.38 (s, 12H), 1.38-1.31 (s, 12H)

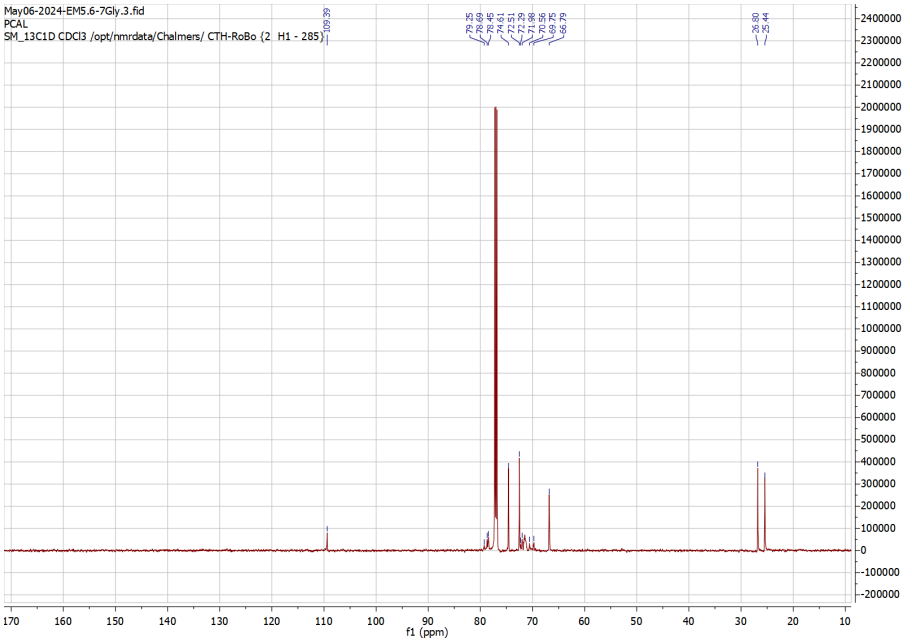

Figure 7.18: ^{13}C NMR spectrum of heptaglycerol ketal in $CDCl_3$.

^{13}C NMR (151 MHz, $CDCl_3$) δ 109.39, 79.25, 78.69, 78.45, 74.61, 72.51, 72.29, 71.98, 70.56, 69.75, 66.79, 26.80, 25.44.

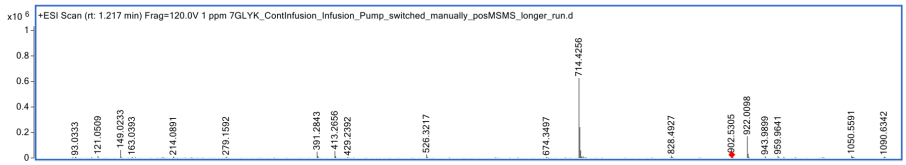

Figure 7.19: Mass spectrum of heptaglycerol ketal. Main ion corresponds to NH4+ adduct of heptaglycerol ketal.

m/z = 714.4256 C33H60O15NH4+ (calculated = 714.427599)

7.5 Heptaglycerol ketal C14 ester

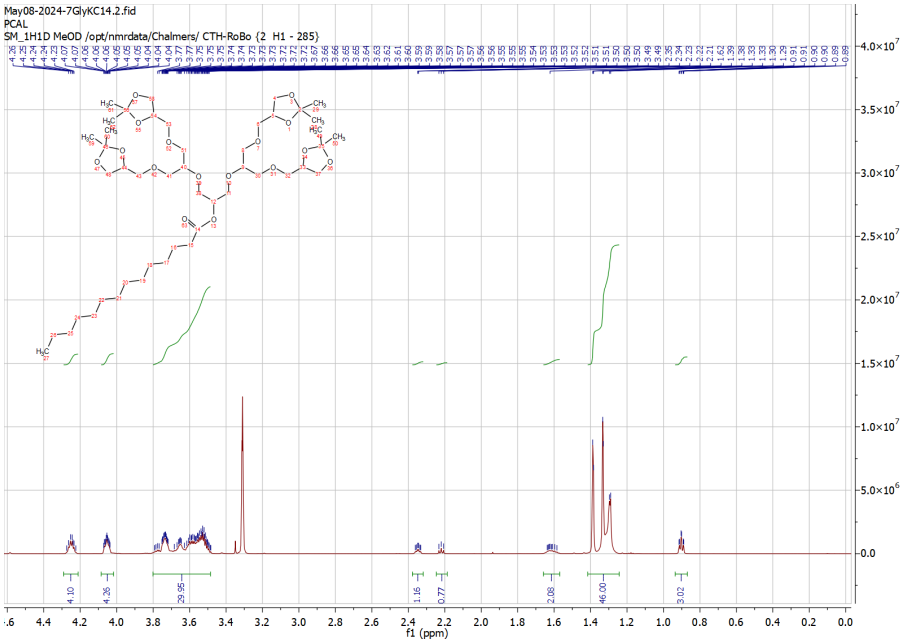

Figure 7.20: ^{1}H NMR spectrum of heptaglycerol ketal C14 ester in MeOD.

^{1}H NMR (600 MHz, MeOD) δ 4.29-4.21 (m, 4H), 4.09-4.01 (t, 4H), 3.80-3.49 (m, 30H), 2.38-2.32 (m, 1H), 2.25-2.18 (t, 1H), 1.41-1.24 (s+s+m overlapping), 46H), 0.92-0.87 (t,3H)

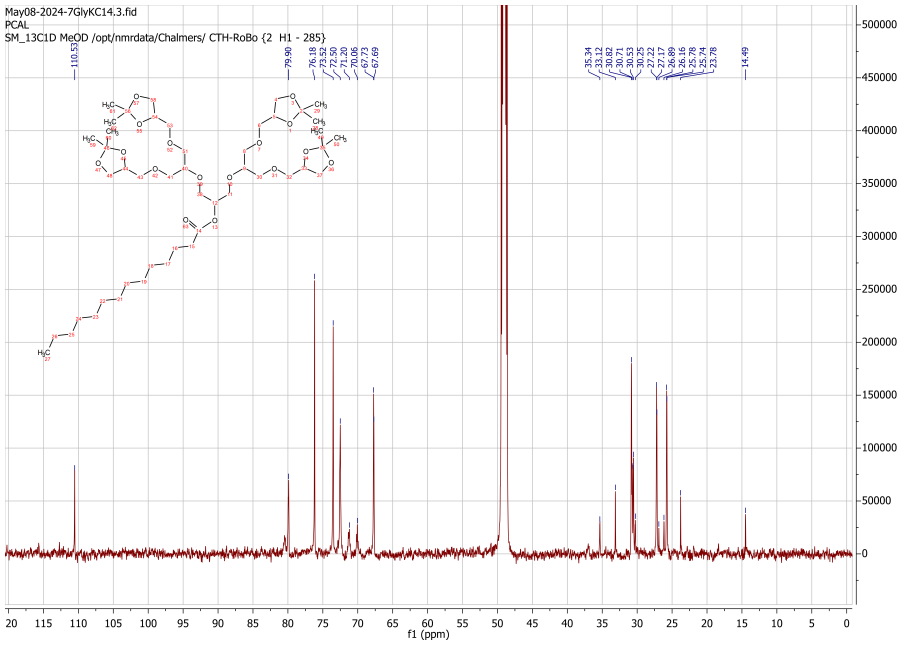

Figure 7.21: ^{13}C NMR spectrum of heptaglycerol ketal C14 ester in MeOD.

^{13}C NMR (151 MHz, MeOD) δ 110.53, 79.90, 76.18, 73.52, 72.50, 71.20, 70.06, 67.73, 67.69, 35.34, 33.12, 30.82, 30.71, 30.53, 30.25, 27.22, 27.17, 26.89, 26.16, 25.78, 25.74, 23.78, 14.49.

7.5.1 Heptaglycerol C14 ester

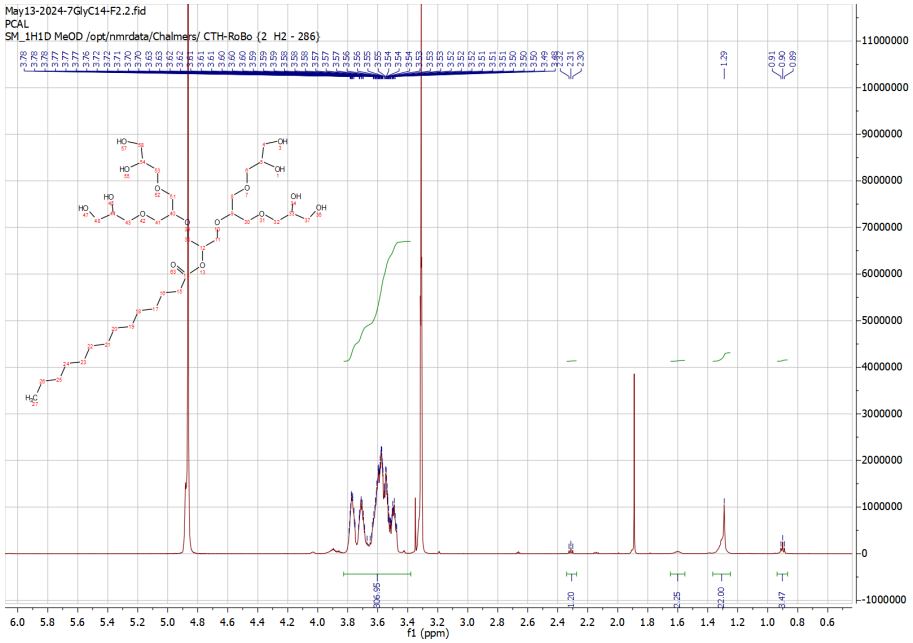

Figure 7.22: ^{1}H NMR spectrum of heptaglycerol C14 ester in MeOD.

^{1}H NMR (600 MHz, MeOD) δ 3.81-3.73 (m, 307H) 2.34-2.27 (t, 1H) 1.65-1.54 (m, 2H) 1.37-1.24 (m, 22H) 0.93-0.87 (t, 3H)

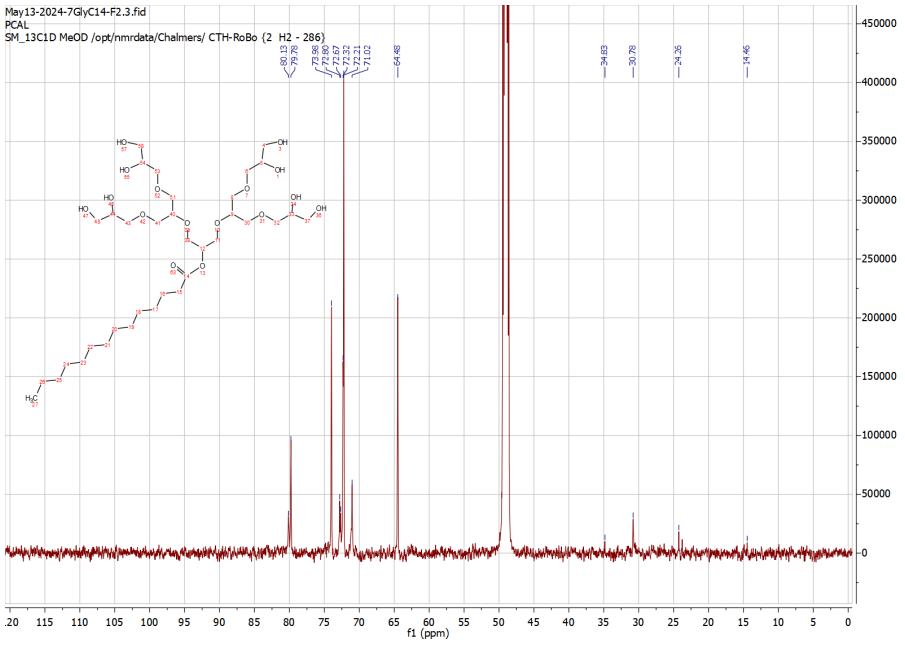

Figure 7.23: ^{13}C NMR spectrum of heptaglycerol C14 ester in MeOD.

^{13}C NMR (151 MHz, MeOD) δ 80.13, 79.78, 73.98, 72.80, 72.67, 72.32, 72.21, 71.02, 64.48, 34.83, 30.78, 24.26, 14.46.

Department of Chemistry and Chemical Engineering
CHALMERS UNIVERSITY OF TECHNOLOGY
Gothenburg, Sweden
www.chalmers.se

CHALMERS
UNIVERSITY OF TECHNOLOGY